

Deviation to the Tri-Bi-Maximal flavor pattern and equivalent classes

E. Barradas-Guevara,^{1,*} O. Félix-Beltrán,^{2,†} and F. Gonzalez-Canales^{2,‡}

¹*Facultad de Ciencias Físico Matemáticas, Benemérita Universidad Autónoma de Puebla,
Apdo. Postal 1152, Puebla, Pue. 72000, México.*

²*Facultad de Ciencias de la Electrónica, Benemérita Universidad Autónoma de Puebla,
Apdo. Postal 542, Puebla, Pue. 72000, México.*

(Dated: April 11, 2022)

In the model-independent context, where the neutrino mass matrix is assumed to be diagonalized by means of a unitary matrix that possess the Tri-Bi-Maximal (TBM) flavor mixing pattern. We present an analysis where the TBM deviation is explored by considering different forms, with texture zeros, for the charged lepton mass matrix. These last mass matrices are classified into equivalent classes. We are interested in the charged lepton mass matrices with the minimum free parameter number, *i.e.* the maximum number of texture zeros, that allows us to correctly reproduce the reactor mixing angle value. We show a deviation from the TBM pattern in terms of the charged lepton masses as well as the theoretical expressions and their parameter space for the mixing angles. Finally, we present the phenomenological implications of numerical values of the “Majorana-like” phase factors on the neutrinoless double-beta decay.

PACS numbers:

I. INTRODUCTION

Although the discovery of masses and flavor mixing of the neutrino can be regarded as one of the biggest breakthroughs in the understanding of particle physics, since it was the first evidence in favor of a beyond the Standard Model physics (BSM) [1]. The experimental discovery of a nonzero reactor mixing angle [2–4] marked the beginning of a new era in particle physics. For these experimental results have expanded the flavor structure in the lepton sector by providing us the first indication for a new CP violation source [5].

However, neutrino oscillation experiments do not resolve the question of whether neutrinos are Majorana or Dirac particles, or give us information about the absolute neutrino mass scale, nor about Majorana phase factors. Majorana phases enter in decay amplitudes that violate the leptonic number, such as neutrinoless double beta decay [6]. Therefore, an experimental observation of neutrinoless double-beta decay can test the absolute scale of neutrinos masses and the nature of the neutrino mass term, *i.e.*, the neutrinos would be Majorana particles. Now it is well known that neutrinos have a small value for their masses, less than eV, which naturally can be explained by considering neutrinos as Majorana particles [7].

*Electronic address: barradas@fcfm.buap.mx

†Electronic address: olga.felix@correo.buap.mx

‡Electronic address: felix.gonzalez@correo.buap.mx

The Tri-bi-maximal mixing pattern (TBM) [8] considers a maximal atmospheric mixing angle $\theta_{23} = 45^\circ$ and solar angle $\theta_{12} \approx 35.26^\circ$, while the reactor angle is postulated as zero. Also, in the TBM framework, the charged lepton mass matrix is considered a diagonal matrix. The TBM flavor pattern was ruled out by the experimental measurement of the reactor angle, which reports a reactor mixing angle of the order of eight degrees [2–4]. However, all is not lost with respect to the TBM pattern, if we remember that the leptonic mixing matrix, PMNS, arises from the mismatch between diagonalization of the mass matrices of charged leptons and the left-handed neutrinos. Realistic Tri-bi-maximal-like Neutrino Mixing Matrix [9, 10].

A generalization can be proposed in which the unitary matrix diagonalizing to the neutrino mass matrix is represented by the TBM flavor pattern, while the unitary matrix that diagonalizes to the charged lepton mass matrix corresponds to corrections to the reactor, solar and atmospheric mixing angles.

This work is structured as follows. In section II we make a brief discussion on the leptonic flavor mixing matrix and its parametrization, the TBM lepton flavor pattern, and neutrinoless double beta decay. In section III we present a framework where the corrections to the TBM pattern come from the charged lepton mass matrix. These last mass matrices are classified into equivalent classes and parameterized in terms of the charged lepton masses. In addition, the allowed regions for the leptonic flavor mixing angles and neutrinoless double beta decay are shown. Finally, in the section IV we provide a brief sum-up discussion at the end.

II. PRELIMINARIES

In the particular case of considering neutrinos as Majorana particles, the low energy neutrino oscillation phenomenon is described by the Lagrangian [11]

$$\mathcal{L} = -\frac{g}{\sqrt{2}}\bar{\ell}_L\gamma^\mu\nu_L W_\mu - \frac{1}{2}\bar{\nu}_R^c\mathbf{M}_\nu\nu_L - \bar{\ell}_R\mathbf{M}_\ell\ell_L + \text{H. c.}, \quad (1)$$

which is written at the base of the flavor eigenstates. In this Lagrangian the first term corresponds to the charged currents, the second is a Majorana mass term for neutrinos, and the third part corresponds to the charged lepton mass term. Thus, the \mathbf{M}_ν is the neutrino mass matrix, while \mathbf{M}_ℓ is the charged lepton mass matrix. As well, the \mathbf{M}_ν is the neutrino mass matrix which is a 3×3 complex symmetric matrix, while \mathbf{M}_ℓ is the charged lepton mass matrix which, in general, is a 3×3 complex mass matrix. The matrices in eq. (1) can be rotated to the mass eigenstates basis by means of the unitary transformations

$$\mathbf{M}_\nu = \mathbf{U}_\nu^* \mathbf{\Delta}_\nu \mathbf{U}_\nu^\dagger \quad \text{and} \quad \mathbf{M}_\ell = \mathbf{V}_\ell \mathbf{\Delta}_\ell \mathbf{U}_\ell^\dagger. \quad (2)$$

On this basis the mass matrices have the diagonal form, $\mathbf{\Delta}_\nu = \text{diag}(m_{\nu 1}, m_{\nu 2}, m_{\nu 3})$ and $\mathbf{\Delta}_\ell = \text{diag}(m_e, m_\mu, m_\tau)$. The unitary matrices in eq. (2) are obtained from the singular value decomposition theorem. From eqs. (1) and (2) the charged currents term takes the form

$$\mathcal{L}_{cc} = \bar{\ell}'_L \gamma^\mu \mathbf{U}_{\text{PMNS}} \nu'_L, \quad (3)$$

where $\ell'_L = \mathbf{U}_\ell \ell_L$, $\nu'_L = \mathbf{U}_\nu \nu_L$, and

$$\mathbf{U}_{\text{PMNS}} = \mathbf{U}_\ell^\dagger \mathbf{U}_\nu = \begin{pmatrix} U_{e1} & U_{e2} & U_{e3} \\ U_{\mu 1} & U_{\mu 2} & U_{\mu 3} \\ U_{\tau 1} & U_{\tau 2} & U_{\tau 3} \end{pmatrix}. \quad (4)$$

The last expression is the leptonic flavor mixing matrix, which is known as the PMNS matrix and governs the neutrinos and lepton couplings. In the symmetric parametrization the leptonic flavor mixing matrix has the form [12]

$$\begin{pmatrix} c_{12}c_{13} & s_{12}c_{13}e^{-i\phi_{12}} & s_{13}e^{-i\phi_{13}} \\ -s_{12}c_{23}e^{i\phi_{12}} - c_{12}s_{13}s_{23}e^{-i(\phi_{23}-\phi_{13})} & c_{23}c_{12} - s_{23}s_{12}s_{13}e^{-i(\phi_{12}+\phi_{23}-\phi_{13})} & c_{13}s_{23}e^{-i\phi_{23}} \\ s_{12}s_{23}e^{i(\phi_{12}+\phi_{23})} - c_{12}s_{13}c_{23}e^{i\phi_{13}} & -c_{12}s_{23}e^{i\phi_{23}} - s_{12}s_{13}c_{23}e^{-i(\phi_{12}-\phi_{13})} & c_{13}c_{23} \end{pmatrix}, \quad (5)$$

where $c_{ij} = \cos \theta_{ij}$, $s_{ij} = \sin \theta_{ij}$, and $\phi_{12}, \phi_{13}, \phi_{23}$ are the physical phases. The symmetric and PDG [6] parametrization are related each other by means $\mathbf{U}_{\text{PDG}} = \mathbf{K}\mathbf{U}_{\text{sym}}$, where $\mathbf{K} = \text{diag}(1, e^{i\beta_1/2}, e^{i\beta_2/2})$ with the phase factors $\beta_1 = -2\phi_{12}$, $\beta_2 = -2(\phi_{12} + \phi_{23})$, and $\delta_{\text{CP}} = \phi_{13} - \phi_{23} - \phi_{12}$ [13]. The mixing angles in terms of the PMNS matrix entries are

$$\sin^2 \theta_{12} = \frac{|U_{e2}|^2}{1-|U_{e3}|^2}, \quad \sin^2 \theta_{23} = \frac{|U_{\mu 3}|^2}{1-|U_{e3}|^2}, \quad \text{and} \quad \sin^2 \theta_{13} = |U_{e3}|^2. \quad (6)$$

While the phase factors associated with the CP violation phases are:

$$\sin \delta_{\text{CP}} = \frac{\mathcal{J}_{\text{CP}}(1-|U_{e3}|^2)}{|U_{e1}||U_{e2}||U_{e3}||U_{\mu 3}||U_{\tau 3}|}, \quad \sin(-2\phi_{12}) = \frac{\mathcal{I}_1}{|U_{e1}|^2|U_{e2}|^2}, \quad \text{and} \quad \sin(-2\phi_{13}) = \frac{\mathcal{I}_2}{|U_{e1}|^2|U_{e3}|^2}, \quad (7)$$

where $\mathcal{J}_{\text{CP}} = \mathbb{I}m \{U_{e3}U_{\mu 3}^*U_{e1}^*U_{\mu 1}\}$ is the Jarlskog invariant which is associated with the CP violation phase Dirac-like. Also, $\mathcal{I}_1 = \mathbb{I}m \{|U_{e1}|^2|U_{e2}|^2\}$ and $\mathcal{I}_2 = \mathbb{I}m \{|U_{e1}|^2|U_{e3}|^2\}$ are the invariants associated with the CP violation phase factors Majorana-like [13].

A. The TBM leptonic flavor pattern

In the framework of TBM flavor mixing pattern the charged lepton mass matrix has a diagonal form, while the solar, atmospheric and reactor mixing angles have the values $\sin^2 \theta_{12} = \frac{1}{2}$, $\theta_{23} = \frac{\pi}{4}$, and $\theta_{13} = 0$, respectively. Furthermore, the CP symmetry is preserved, this means that phase factors are null. Consequently, the unitary matrix \mathbf{U}_ℓ is equal to identity matrix, and the PMNS matrix has the form $\mathbf{U}_{\text{TBM}} = \mathbf{U}_{\text{PMNS}} = \mathbf{U}_\nu$ [8, 14],

$$\mathbf{U}_{\text{TBM}} = \begin{pmatrix} \sqrt{\frac{2}{3}} & \frac{1}{\sqrt{3}} & 0 \\ -\frac{1}{\sqrt{6}} & \frac{1}{\sqrt{3}} & \frac{1}{\sqrt{2}} \\ \frac{1}{\sqrt{6}} & -\frac{1}{\sqrt{3}} & \frac{1}{\sqrt{2}} \end{pmatrix}. \quad (8)$$

In this scheme, the neutrino mass matrix has the form

$$\mathbf{M}_\nu = \begin{pmatrix} b_\nu & a_\nu & -a_\nu \\ a_\nu & b_\nu + d_\nu & b_\nu + c_\nu \\ -a_\nu & b_\nu + c_\nu & b_\nu + d_\nu \end{pmatrix}, \quad (9)$$

where $a_\nu = \frac{1}{3}(m_{\nu 2} - m_{\nu 1})$, $b_\nu = \frac{1}{3}(2m_{\nu 1} + m_{\nu 2})$, $c_\nu = \frac{1}{2}(m_{\nu 3} - \frac{4}{3}m_{\nu 2} - \frac{5}{3}m_{\nu 1})$, and $d_\nu = \frac{1}{2}(m_{\nu 3} - m_{\nu 1})$.

Unfortunately, in agreement with the current experimental data on neutrino oscillations, the TBM leptonic flavor pattern can not done correct description of nature, since the reactor mixing angle is non null. Also, there is a mount of evidences for CP violation in neutrino oscillations. From the current results obtained in a global fit of neutrino oscillation data in the simplest three neutrino theoretical framework, for a normal and inverted hierarchy, we have

the following numerical values for the neutrino oscillation parameters at the best fit point $\pm 1\sigma$ and 3σ [5]:

$$\begin{aligned} \Delta m_{21}^2 (10^{-5} \text{ eV}^2) &= 7.50_{-0.20}^{+0.22}, \quad 6.94 - 8.14, \\ |\Delta m_{31}^2| (10^{-3} \text{ eV}^2) &= \begin{cases} 2.55_{-0.03}^{+0.02}, & 2.47 - 2.63, & \text{for NH,} \\ 2.45_{-0.03}^{+0.02}, & 2.37 - 2.53, & \text{for IH,} \end{cases} \end{aligned} \quad (10)$$

$$\begin{aligned} \sin^2 \theta_{12} (10^{-1}) &= 3.18 \pm 0.16, \quad 2.71 - 3.69, \\ \sin^2 \theta_{23} (10^{-1}) &= \begin{cases} 5.74 \pm 0.14, & 4.34 - 6.10, & \text{for NH,} \\ 5.78_{-0.17}^{+0.10}, & 4.33 - 6.08, & \text{for IH,} \end{cases} \\ \sin^2 \theta_{13} (10^{-2}) &= \begin{cases} 2.200_{-0.062}^{+0.069}, & 2.000 - 2.405 & \text{for NH,} \\ 2.225_{-0.070}^{+0.064}, & 2.018 - 2.424 & \text{for IH.} \end{cases} \end{aligned} \quad (11)$$

In the above expressions $\Delta m_{ij}^2 = m_{\nu_i}^2 - m_{\nu_j}^2$ and NH and IH denote the normal and inverted hierarchy in the neutrino mass spectrum, respectively.

B. Neutrinoless double-beta decay

The neutrinoless double beta decay ($0\nu\beta\beta$) is a second-order process in which a nucleus decays into another by the emission of two electrons [15],

$$(A, Z) \rightarrow (A, Z + 2) + e^- + e^-. \quad (12)$$

This hypothesized nuclear transition is forbidden in the theoretical framework of the Standard Model. Consequently, the study of all variations of $0\nu\beta\beta$ is equally interesting for investigating the so-called new particle physics (NPP). The experimental discovery of one of these processes could solve the open question about the absolute value of neutrino masses and their hierarchy on the mass spectrum. Moreover, the $0\nu\beta\beta$ could be a fundamental tool to study neutrino physics, since this nuclear transition only exists if neutrinos are Majorana particles, which means that it would be the first signal of the non-conservation of the lepton number. The amplitude for ($0\nu\beta\beta$) is proportional to the Majorana effective mass [16]

$$m_{ee} = \sum_i m_{\nu_i} U_{ei}^2, \quad i = 1, 2, 3, \quad (13)$$

where m_{ν_i} ($i = 1, 2, 3$) are the Majorana neutrino masses and U_{ei} the elements of the first row of leptonic flavor mixing matrix PMNS, eq. (4). In the symmetric parametrization of leptonic flavor mixing matrix, eq. (5), the Majorana effective mass has the form

$$|m_{ee}| = |m_{\nu_1} c_{12}^2 c_{13}^2 + m_{\nu_2} s_{12}^2 c_{13}^2 e^{-i2\phi_{12}} + m_{\nu_3} s_{13}^2 e^{-i2\phi_{13}}|, \quad (14)$$

where ϕ_{12} and ϕ_{13} are the Majorana phase factor given in eq. (7). In the above expression the m_{ν_i} neutrino masses can be written in terms of the lightest neutrino mass through the expressions

$$m_{\nu_{3[2]}} = \sqrt{m_{\nu_{1[3]}} + \Delta m_{31[23]}^2} \quad \text{and} \quad m_{\nu_{2[1]}} = \sqrt{m_{\nu_{1[3]}} + \Delta m_{21[31]}^2}, \quad (15)$$

where $m_{\nu_{1[3]}}$ is the lightest neutrino mass for the normal[inverted] hierarchy in the neutrino mass spectrum. Additionally, the mass $m_{\nu_{1[3]}}$ is considered as the only free parameter in the effective mass m_{ee} .

III. DEVIATIONS FROM THE TBM FLAVOR PATTERN

A possible modification to the TBM flavor pattern may come from the charged lepton sector to considering the mass matrix of these without a diagonal form. In this generalization of TBM pattern, the neutrino mass matrix is given by eq. (9), whereas to fix the form of the charged lepton mass matrix, we propose several equivalence classes whose elements are Hermitian matrices with two texture zeros. These Hermitian matrices may be written as

$$\mathbf{M}_\ell^i = \mathbf{U}_\ell^i \mathbf{\Delta}_\ell \mathbf{U}_\ell^{i\dagger}, \quad (16)$$

where

$$\mathbf{U}_\ell^i = \mathbf{T}_i \mathbf{P}_\ell^\dagger \mathbf{O}_\ell, \quad i = 0, \dots, 5. \quad (17)$$

In this expression, the \mathbf{T}_i are the elements of S_3 real representation, see eq. (A1), \mathbf{P}_ℓ is the diagonal matrix of phase factors, which is obtained when the charged lepton mass matrix is written in a polar form, and \mathbf{O}_ℓ is a real orthogonal matrix whose explicit form is different for each equivalent class.

From eqs. (4), (8) and (17) the PMNS matrix takes the form

$$\mathbf{U}_{\text{PMNS}}^i = \mathbf{U}_\ell^{i\dagger} \mathbf{U}_\nu = \mathbf{O}_\ell^\top \mathbf{P}_\ell \mathbf{T}_i \mathbf{U}_{\text{TBM}}. \quad (18)$$

The explicit form of the \mathbf{O}_ℓ and \mathbf{P}_ℓ matrices depends on the equivalence class and the number of texture zeros it contains. Before moving on to define the rule under which texture zeros in a matrix are counted. The rule is; one texture-zero on the diagonal counts as one, while two off-diagonal counts as one texture zero [17, 18].

A. Equivalent class with two texture zeros type-I

The equivalent class for Hermitian matrices with two texture zeros type-I have the form [18]:

$$\begin{aligned} \mathbf{M}_\ell^0 &= \begin{pmatrix} 0 & a_\ell & 0 \\ a_\ell^* & b_\ell & c_\ell \\ 0 & c_\ell^* & d_\ell \end{pmatrix}, \quad \mathbf{M}_\ell^1 = \begin{pmatrix} b_\ell & a_\ell^* & c_\ell \\ a_\ell & 0 & 0 \\ c_\ell^* & 0 & d_\ell \end{pmatrix}, \quad \mathbf{M}_\ell^2 = \begin{pmatrix} d_\ell & c_\ell^* & 0 \\ c_\ell & b_\ell & a_\ell^* \\ 0 & a_\ell & 0 \end{pmatrix}, \\ \mathbf{M}_\ell^3 &= \begin{pmatrix} 0 & 0 & a_\ell \\ 0 & d_\ell & c_\ell^* \\ a_\ell^* & c_\ell & b_\ell \end{pmatrix}, \quad \mathbf{M}_\ell^4 = \begin{pmatrix} d_\ell & 0 & c_\ell^* \\ 0 & 0 & a_\ell \\ c_\ell & a_\ell^* & b_\ell \end{pmatrix}, \quad \mathbf{M}_\ell^5 = \begin{pmatrix} b_\ell & c_\ell & a_\ell^* \\ c_\ell^* & d_\ell & 0 \\ a_\ell & 0 & 0 \end{pmatrix}, \end{aligned} \quad (19)$$

where $d_\ell = 1 - \delta_\ell$,

$$a_\ell = \sqrt{\frac{\tilde{m}_e \tilde{m}_\mu}{1 - \delta_\ell}} e^{i\phi_a}, \quad b_\ell = (\mathbf{s}_3 - 1) + \mathbf{s}_1 \tilde{m}_e + \mathbf{s}_2 \tilde{m}_\mu + \delta_\ell, \quad c_\ell = \sqrt{\frac{f_{\ell 1} f_{\ell 2} f_{\ell 3}}{1 - \delta_\ell}} e^{i\phi_c}, \quad (20)$$

with $f_{\ell 1} = 1 - \mathbf{s}_1 \tilde{m}_e - \delta_\ell$, $f_{\ell 2} = \mathbf{s}_3 (1 - \mathbf{s}_2 \tilde{m}_\mu - \delta_\ell)$, $f_{\ell 3} = 1 + \mathbf{s}_3 (\delta_\ell - 1)$, $\tilde{m}_e = \frac{m_e}{m_\tau}$, $\tilde{m}_\mu = \frac{m_\mu}{m_\tau}$, $\phi_a = \arg\{a_\ell\}$, and $\phi_c = \arg\{c_\ell\}$. These last two expressions correspond to the phase factors of the complex mass matrix elements, which are related to the CP violation and are defined in the open-close interval $(-\pi, \pi]$. In this case, the diagonal matrix of phase factors is $\mathbf{P}_\ell = \text{diag}(1, e^{i\phi_a}, e^{i(\phi_a + \phi_c)})$. The real orthogonal matrix \mathbf{O}_ℓ is constructed with the help of the

general eigenvectors given in eq. (B2), which are the eigenvectors of the charged lepton mass matrix. The explicit form of $\mathbf{O}_\ell = (|M_1\rangle, |M_2\rangle, |M_3\rangle)$ is

$$\mathbf{O}_\ell = \begin{pmatrix} \mathbf{s}_1 \sqrt{\frac{\tilde{m}_\mu f_{\ell 1}}{D_{\ell 1}}} & \mathbf{s}_2 \sqrt{\frac{\tilde{m}_e f_{\ell 2}}{D_{\ell 2}}} & \mathbf{s}_3 \sqrt{\frac{\tilde{m}_e \tilde{m}_\mu f_{\ell 3}}{D_{\ell 3}}} \\ \sqrt{\frac{\tilde{m}_e (1-\delta_\ell) f_{\ell 1}}{D_{\ell 1}}} & \sqrt{\frac{\tilde{m}_\mu (1-\delta_\ell) f_{\ell 2}}{D_{\ell 2}}} & \sqrt{\frac{(1-\delta_\ell) f_{\ell 3}}{D_{\ell 3}}} \\ -\sqrt{\frac{\tilde{m}_e f_{\ell 2} f_{\ell 3}}{D_{\ell 1}}} & \mathbf{s}_1 \mathbf{s}_2 \sqrt{\frac{\tilde{m}_\mu f_{\ell 1} f_{\ell 3}}{D_{\ell 2}}} & \mathbf{s}_3 \sqrt{\frac{f_{\ell 1} f_{\ell 2}}{D_{\ell 3}}} \end{pmatrix}, \quad (21)$$

where

$$\begin{aligned} D_{\ell 1} &= (1 - \delta_\ell) (\tilde{m}_\mu + \mathbf{s}_3 \tilde{m}_e) (1 + \mathbf{s}_2 \tilde{m}_e), & D_{\ell 2} &= (1 - \delta_\ell) (\tilde{m}_\mu + \mathbf{s}_3 \tilde{m}_e) (1 + \mathbf{s}_1 \tilde{m}_\mu), \\ D_{\ell 3} &= (1 - \delta_\ell) (1 + \mathbf{s}_2 \tilde{m}_e) (1 + \mathbf{s}_1 \tilde{m}_\mu). \end{aligned} \quad (22)$$

In the last expressions $\mathbf{s}_k = \text{sign}(m_{\ell k})$ with $k = 1, 2, 3$, which means that we must consider that $m_{\ell k} = -m_{\ell k}$ to avoid a sign inconsistency in the expression of a_ℓ , which could cause this to be a purely imaginary amount. For charged lepton fields the sign of the mass is irrelevant since the sign can be changed by means of the chiral transformations; $\ell_R \rightarrow \ell'_R = e^{i\gamma_5 \frac{\pi}{2}} \ell_R$ and $\ell_L \rightarrow \ell'_L = e^{i\gamma_5 \frac{\pi}{2}} \ell_L$. These transformations change the sign of the eigenvalues, however, the rest of the Lagrangian keeps invariant. The parameter δ_ℓ must satisfy the conditions

$$\begin{aligned} \textbf{A.} \quad & 0 < \delta_\ell < 1 - \tilde{m}_\mu, & \text{for} \quad & m_e = -m_e \quad (\mathbf{s}_1 = -1, \mathbf{s}_2 = +1, \mathbf{s}_3 = +1). \\ \textbf{B.} \quad & 0 < \delta_\ell < 1 - \tilde{m}_e, \quad \delta_\ell \neq \tilde{m}_\mu - \tilde{m}_e, & \text{for} \quad & m_\mu = -m_\mu \quad (\mathbf{s}_1 = +1, \mathbf{s}_2 = -1, \mathbf{s}_3 = +1). \\ \textbf{C.} \quad & 1 - \tilde{m}_\mu < \delta_\ell < 1 - \tilde{m}_e, & \text{for} \quad & m_\tau = -m_\tau \quad (\mathbf{s}_1 = +1, \mathbf{s}_2 = +1, \mathbf{s}_3 = -1). \end{aligned} \quad (23)$$

In this case, the flavor mixing angles in eq. (6) have the form:

$$\sin^2 \theta_{12} = \frac{1}{3} \frac{\tilde{m}_e}{\tilde{m}_\mu} \varepsilon_{12}, \quad \sin^2 \theta_{23} = \frac{1}{2} \frac{(1+\mathbf{s}_2 \tilde{m}_e)}{(1+\mathbf{s}_1 \tilde{m}_\mu)} \varepsilon_{23}, \quad \sin^2 \theta_{13} = \frac{1}{2} \frac{\tilde{m}_e}{\tilde{m}_\mu} \varepsilon_{13}. \quad (24)$$

The explicit form of the ε_{ij} parameters is given in the Appendix C 1. From the allowed regions of flavor mixing angles shown in the figure 1, which are computed taken into account the condition **B** (23) it is easy to conclude that all charged lepton mass matrices are able to reproduce the current experimental values of reactor, solar and atmospheric angles. However, the numerical values interval of the free parameter δ_ℓ , for the \mathbf{M}_ℓ^1 , \mathbf{M}_ℓ^2 , \mathbf{M}_ℓ^4 and \mathbf{M}_ℓ^5 mass matrices, is too small. Consequently, for this equivalent class, to reproduce the values for the leptonic flavor mixing angles, at 3σ obtained from the global fit eq. (11), for a normal (NH) and inverted (IH) hierarchy. The free parameter δ_ℓ should be in the following numerical interval:

$$\begin{aligned} \delta_\ell &\in [0.99132, 0.99382] && \text{for } \mathbf{M}_\ell^0 \text{ and } \mathbf{M}_\ell^3, \\ \delta_\ell &\approx 0.9994 && \text{for } \mathbf{M}_\ell^1 \text{ and } \mathbf{M}_\ell^5, \\ \delta_\ell &\approx 0.9997 && \text{for } \mathbf{M}_\ell^2 \text{ and } \mathbf{M}_\ell^4. \end{aligned} \quad (25)$$

In this equivalent class, from expressions in Appendix C 1 and figure 2 we conclude, shown:

1. For the mass matrices \mathbf{M}_ℓ^0 and \mathbf{M}_ℓ^3 , on the one hand the expression for solar mixing angle can reproduce the current experimental data independently of numerical value of phase factors ϕ_a and ϕ_c . In other words, the mixing angle θ_{12} has a weak dependence on parameters ϕ_a and ϕ_c . On the other hand, the expression for the mixing angle θ_{13} does not has a explicit dependence on phase factor ϕ_a , but if has a weak dependence on phase

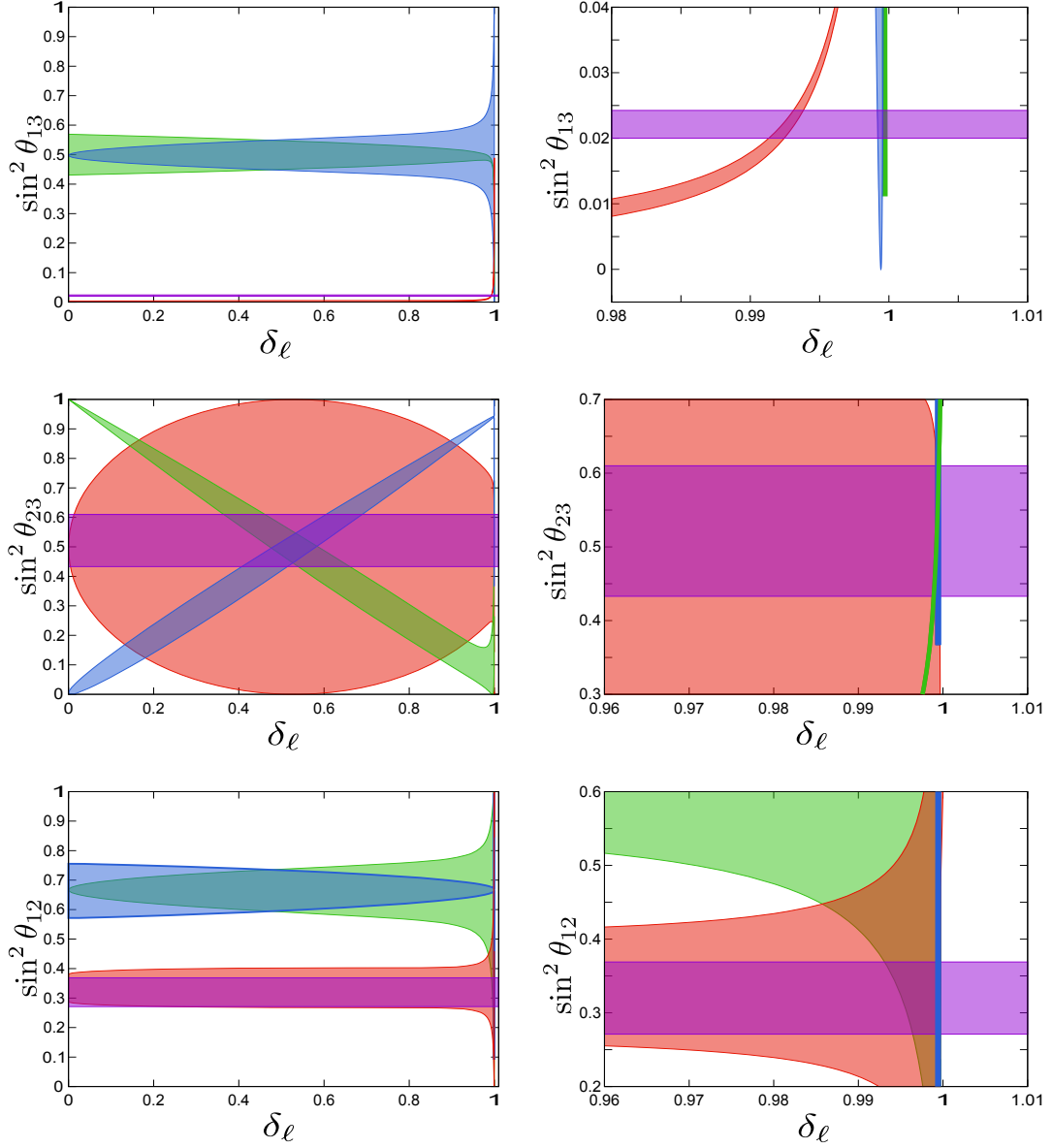


FIG. 1: The allowed regions for the reactor (upper panels), atmospheric (middle panels), and solar (lower panels) mixing angles and free parameter δ_ℓ for equivalent class with two texture zeros type-I. The purple stripe corresponds to the values at 3σ for the reactor, atmospheric and solar mixing angles obtained from the global fit, for normal and inverted hierarchy [5]. In these panels, the red area is for \mathbf{M}_ℓ^0 and \mathbf{M}_ℓ^3 , blue area is for \mathbf{M}_ℓ^1 and \mathbf{M}_ℓ^5 , the green area is for \mathbf{M}_ℓ^2 and \mathbf{M}_ℓ^4 . The right panels show an amplification of the region in which the mixing angles theoretical expressions simultaneously reproduce the current experimental data.

factor ϕ_c . Finally, the expression for the mixing angle θ_{23} does not have an explicit dependence on phase factor ϕ_a . However, to reproduce the current experimental data at 3σ given in eq. (11) for the θ_{23} angle, the phase factor ϕ_c must be on the following numerical interval;

$$|\phi_c| \in [76^\circ, 180^\circ] \quad \text{for } \mathbf{M}_\ell^0 \text{ and } \mathbf{M}_\ell^3. \quad (26)$$

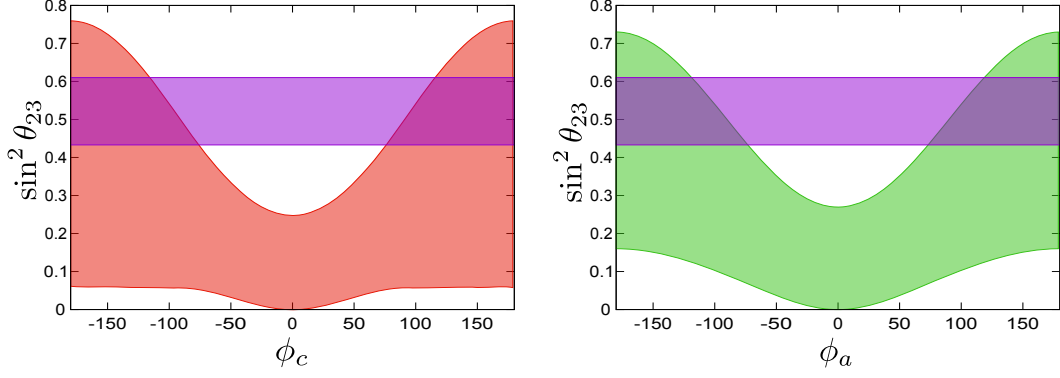


FIG. 2: The allowed regions for the atmospheric mixing angle and free parameters ϕ_a and ϕ_c , for equivalent class with two texture zeros type-I. The purple stripe corresponds to the values at 3σ for atmospheric mixing angle obtained from the global fit, for normal and inverted hierarchy [5]. In these panels, the red area is for \mathbf{M}_ℓ^0 and \mathbf{M}_ℓ^3 , and the green area is for \mathbf{M}_ℓ^2 and \mathbf{M}_ℓ^4 .

2. For the mass matrices \mathbf{M}_ℓ^1 and \mathbf{M}_ℓ^5 , the reactor, solar and atmospheric mixing angles have a weak dependence on the phase factors ϕ_a and ϕ_c .
3. For the mass matrices \mathbf{M}_ℓ^2 and \mathbf{M}_ℓ^4 , on the one hand the expression for the mixing angle θ_{12} has a weak dependence on parameters ϕ_a and ϕ_c . On the other hand, the expression for the mixing angle θ_{13} does not has a explicit dependence on phase factor ϕ_c , but if has a weak dependence on phase factor ϕ_a . Finally, the expression for the mixing angle θ_{23} does not has a explicit dependence on phase factor ϕ_c . So, to reproduce the current experimental data eq. (11) at 3σ for the θ_{23} angle, the phase factor ϕ_a runs over the numerical range

$$|\phi_a| \in [76^\circ, 180^\circ] \text{ for } \mathbf{M}_\ell^2 \text{ and } \mathbf{M}_\ell^4. \quad (27)$$

In figure 3 we show the allowed regions for the magnitude of the Majorana effective mass $|m_{ee}|$, eq. (14), which were obtained in a model-independent context where the neutrino mass matrix has the form given in eq. (9), while the charged lepton matrix is represented for an element of the equivalent class with two texture zeros type-I. eq. (19). Each one of these regions was obtained by considering the values given in eqs. (25)-(27) for the free parameter δ_ℓ constrained by \mathbf{B} (23), and the associated to the CP violation phases ϕ_a and ϕ_c .

B. Equivalent class with two texture zeros type-II

The equivalent class for Hermitian matrices with two texture zeros type-II have the form [18]:

$$\begin{aligned} \mathbf{M}_\ell^0 &= \begin{pmatrix} f_\ell & a_\ell & 0 \\ a_\ell^* & 0 & c_\ell \\ 0 & c_\ell^* & d_\ell \end{pmatrix}, \quad \mathbf{M}_\ell^1 = \begin{pmatrix} 0 & a_\ell^* & c_\ell \\ a_\ell & f_\ell & 0 \\ c_\ell^* & 0 & d_\ell \end{pmatrix}, \quad \mathbf{M}_\ell^2 = \begin{pmatrix} d_\ell & c_\ell^* & 0 \\ c_\ell & 0 & a_\ell^* \\ 0 & a_\ell & f_\ell \end{pmatrix}, \\ \mathbf{M}_\ell^3 &= \begin{pmatrix} f_\ell & 0 & a_\ell \\ 0 & d_\ell & c_\ell^* \\ a_\ell^* & c_\ell & 0 \end{pmatrix}, \quad \mathbf{M}_\ell^4 = \begin{pmatrix} d_\ell & 0 & c_\ell^* \\ 0 & f_\ell & a_\ell \\ c_\ell & a_\ell^* & 0 \end{pmatrix}, \quad \mathbf{M}_\ell^5 = \begin{pmatrix} 0 & c_\ell & a_\ell^* \\ c_\ell^* & d_\ell & 0 \\ a_\ell & 0 & f_\ell \end{pmatrix}, \end{aligned} \quad (28)$$

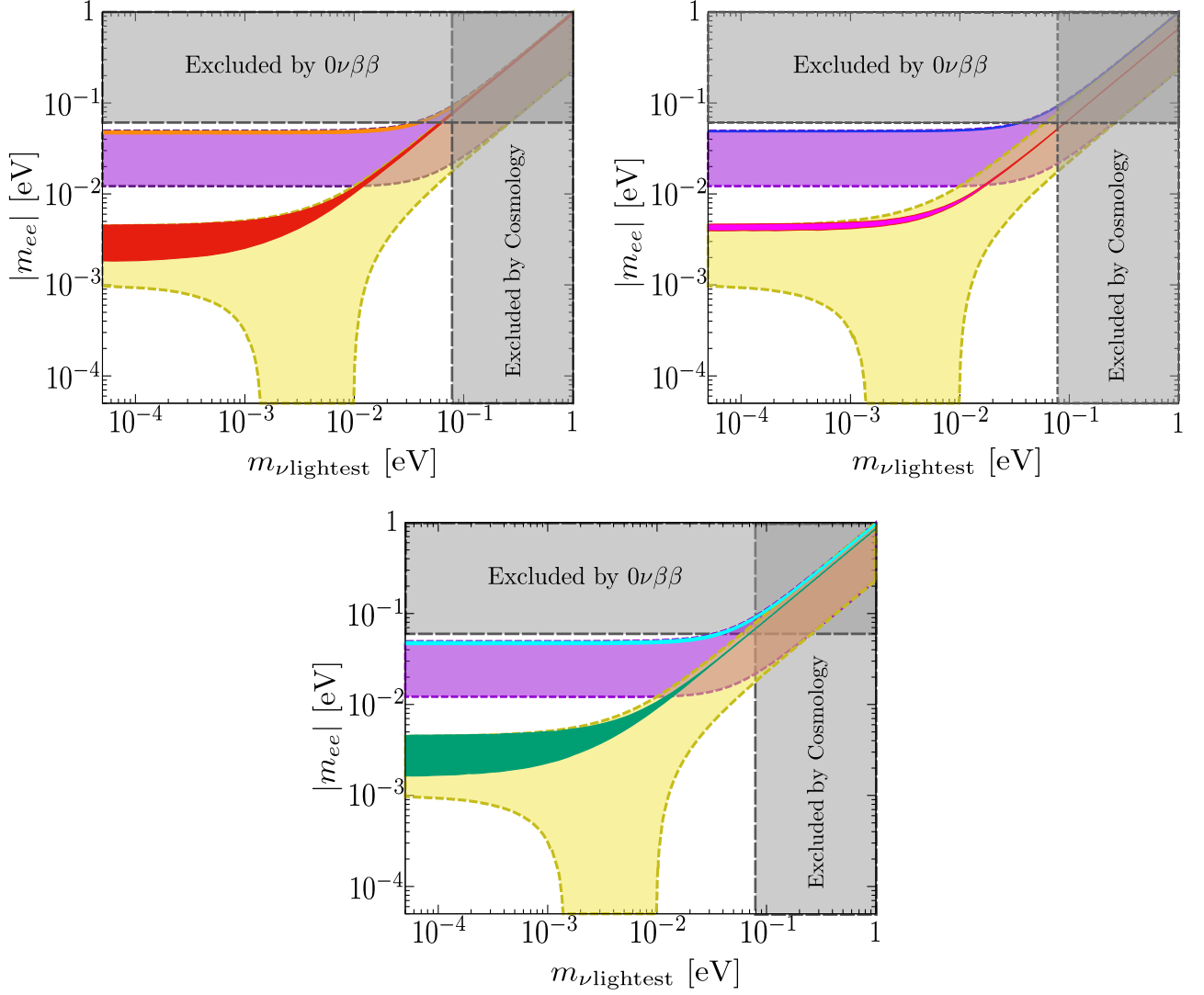


FIG. 3: In these panels, regions allowed for the magnitude of Majorana effective mass $|m_{ee}|$ are shown. Respectively, for an inverted and normal neutrino mass hierarchy, the yellow and purple stripes are obtained from the current experimental data on neutrino oscillations at 3σ [5]. The upper left panel, the red area is for a normal hierarchy while the orange area is for an inverted hierarchy, both areas are obtained from matrices \mathbf{M}_ℓ^0 and \mathbf{M}_ℓ^3 . The upper right panel, the magenta area is for a normal hierarchy while the blue area is for an inverted hierarchy, both areas are obtained from \mathbf{M}_ℓ^1 and \mathbf{M}_ℓ^5 . In the lower panel, the green area is for a normal hierarchy while the cyan area is for an inverted hierarchy, both areas are obtained from \mathbf{M}_ℓ^2 and \mathbf{M}_ℓ^4 . From KamLAND-ZEN [19] and EXO-200 [20] the following upper limit $|m_{ee}| < 0.061$, which correspond to the horizontal grey band. From the results reported by Planck collaboration, obtaining the vertical grey band [21].

where $d_\ell = 1 - \delta_\ell$,

$$a_\ell = \sqrt{\frac{\tilde{\sigma}_{\ell 1} \tilde{\sigma}_{\ell 2} \tilde{\sigma}_{\ell 3}}{\tilde{\mu}_\ell}}, \quad c_\ell = \sqrt{\frac{\delta_\ell f_{\ell 1} f_{\ell 2}}{\tilde{\mu}_\ell}} e^{i\phi_c}, \quad f_\ell = \tilde{m}_e - \tilde{m}_\mu + \delta_\ell, \quad (29)$$

with $\tilde{\sigma}_{\ell 1} = f_\ell - \tilde{m}_e = \delta_\ell - \tilde{m}_\mu$, $\tilde{\sigma}_{\ell 2} = f_\ell + \tilde{m}_\mu = \delta_\ell + \tilde{m}_e$, $\tilde{\sigma}_{\ell 3} = 1 - f_\ell = 1 - \delta_\ell + \tilde{m}_\mu - \tilde{m}_e$, $\tilde{\mu}_\ell = \tilde{m}_e - \tilde{m}_\mu - 1 + 2\delta_\ell$, $f_{\ell 1} = -(1 - \tilde{m}_e - \delta_\ell)$, $f_{\ell 2} = 1 + \tilde{m}_\mu - \delta_\ell$, $f_{\ell 3} = \delta_\ell$, $\phi_a = \arg\{a_\ell\}$, and $\phi_c = \arg\{c_\ell\}$. In this case, the diagonal matrix

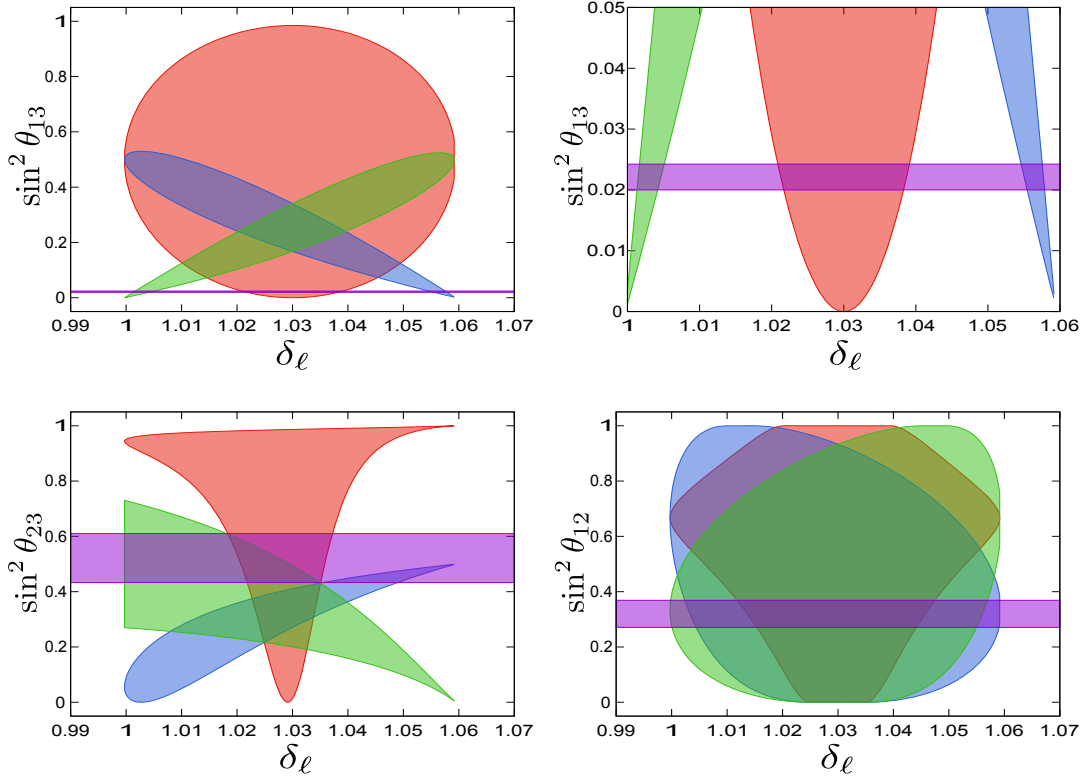


FIG. 4: The allowed regions for the reactor (upper panels), atmospheric, and solar (lower panels) mixing angles and free parameter δ_ℓ , for equivalent class with two texture zeros type-II. The purple stripe corresponds to the values at 3σ for the reactor, atmospheric and solar mixing angles obtained from the global fit, for normal and inverted hierarchy [5]. In these panels, the red area is for \mathbf{M}_ℓ^0 and \mathbf{M}_ℓ^3 , blue area is for \mathbf{M}_ℓ^1 and \mathbf{M}_ℓ^5 , the green area is for \mathbf{M}_ℓ^2 and \mathbf{M}_ℓ^4 . The right lower panel shows an amplification of the region in which the mixing angles theoretical expressions simultaneously reproduce the current experimental data.

of phase factors is $\mathbf{P}_\ell = \text{diag}(1, e^{i\phi_a}, e^{i(\phi_a + \phi_c)})$.

The real orthogonal matrix \mathbf{O}_ℓ is constructed with the help of the general eigenvectors given in eq. (B2), which are the eigenvectors of the charged lepton mass matrix. The explicit form of $\mathbf{O}_\ell = (|M_1\rangle, |M_2\rangle, |M_3\rangle)$ is

$$\mathbf{O}_\ell = \begin{pmatrix} \sqrt{\frac{\tilde{\sigma}_{\ell 2} \tilde{\sigma}_{\ell 3} f_{\ell 1}}{D_{\ell 1}}} & -\sqrt{\frac{\tilde{\sigma}_{\ell 1} \tilde{\sigma}_{\ell 3} f_{\ell 2}}{D_{\ell 2}}} & \sqrt{\frac{\tilde{\sigma}_{\ell 1} \tilde{\sigma}_{\ell 2} f_{\ell 3}}{D_{\ell 3}}} \\ -\sqrt{\frac{\tilde{\sigma}_{\ell 1} \tilde{\mu}_\ell f_{\ell 1}}{D_{\ell 1}}} & \sqrt{\frac{\tilde{\sigma}_{\ell 2} \tilde{\mu}_\ell f_{\ell 2}}{D_{\ell 2}}} & \sqrt{\frac{\tilde{\sigma}_{\ell 3} \tilde{\mu}_\ell f_{\ell 3}}{D_{\ell 3}}} \\ -\sqrt{\frac{\tilde{\sigma}_{\ell 1} \delta_\ell f_{\ell 2}}{D_{\ell 1}}} & -\sqrt{\frac{\tilde{\sigma}_{\ell 2} \delta_\ell f_{\ell 1}}{D_{\ell 2}}} & \sqrt{\frac{\tilde{\sigma}_{\ell 3} f_{\ell 1} f_{\ell 2}}{D_{\ell 3}}} \end{pmatrix}, \quad (30)$$

where

$$\mathcal{D}_{\ell 1} = \tilde{\mu}_\ell (\tilde{m}_\mu + \tilde{m}_e) (1 - \tilde{m}_e), \quad \mathcal{D}_{\ell 2} = \tilde{\mu}_\ell (\tilde{m}_\mu + \tilde{m}_e) (1 + \tilde{m}_\mu), \quad \mathcal{D}_{\ell 3} = \tilde{\mu}_\ell (1 - \tilde{m}_e) (1 + \tilde{m}_\mu). \quad (31)$$

The parameter δ_ℓ must satisfy the conditions

$$1 + \tilde{m}_\mu - \tilde{m}_e > \delta_\ell > 1 - \tilde{m}_e, \quad \text{and} \quad \delta_\ell \neq \tilde{m}_\mu - \tilde{m}_e. \quad (32)$$

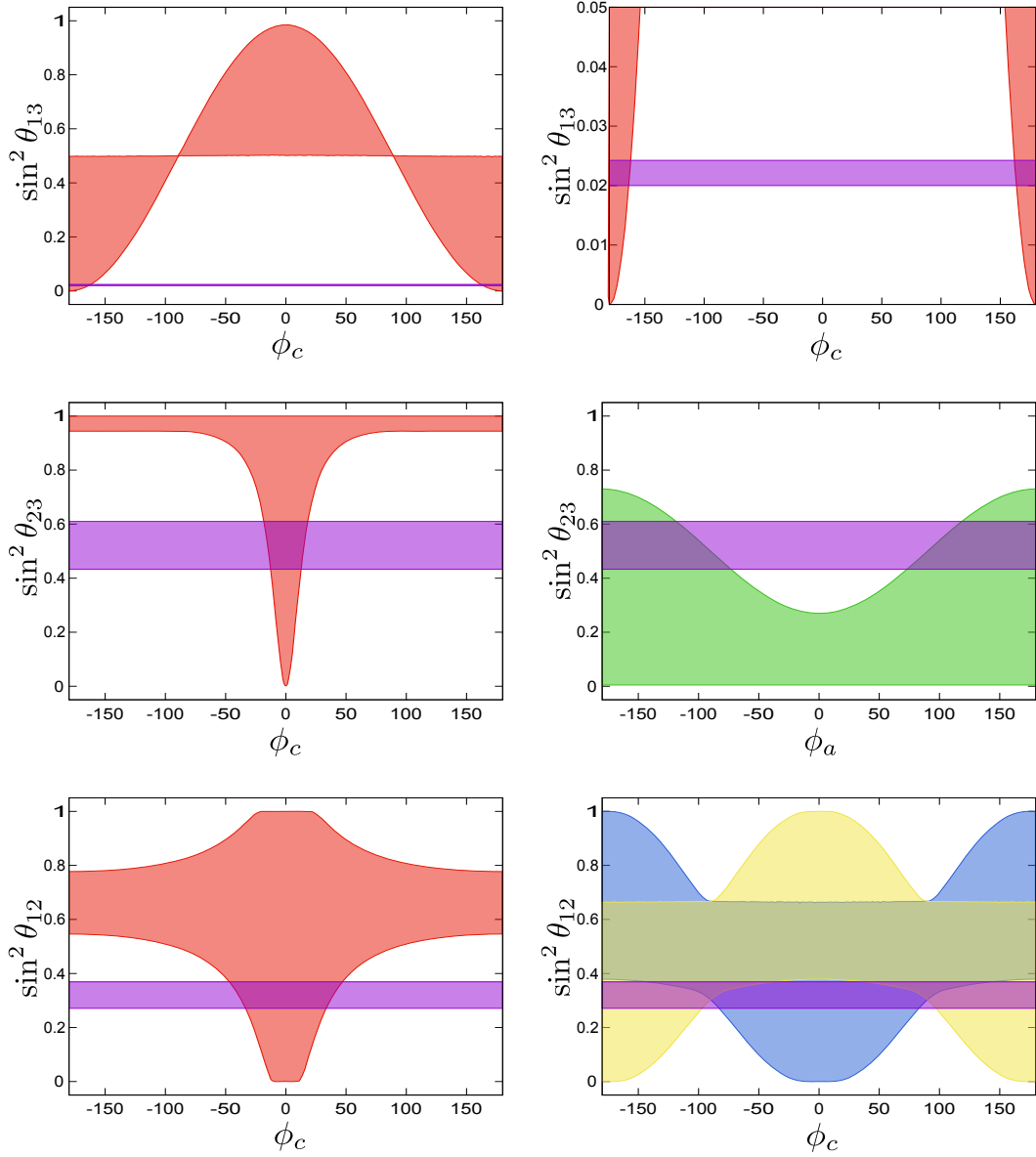


FIG. 5: The allowed regions for the reactor (upper panels), atmospheric (middle panels), and solar (lower panels) mixing angles and free parameters ϕ_a and ϕ_c . The purple stripe corresponds to the values at 3σ for the reactor, solar and atmospheric mixing angles obtained from the global fit, for normal and inverted hierarchy [5]. In these panels, the red area is for \mathbf{M}_ℓ^0 and \mathbf{M}_ℓ^3 , the green area is for \mathbf{M}_ℓ^2 and \mathbf{M}_ℓ^4 , while the blue area is for \mathbf{M}^1 and yellow area is for \mathbf{M}^5 . The right upper panel shows an amplification of the region in which the reactor mixing angle theoretical expression reproduce the current experimental data.

The flavor mixing angles in eq. (6) take the form:

$$\sin^2 \theta_{12} = \frac{1}{3} \frac{\tilde{\sigma}_{\ell 1}}{\tilde{m}_\mu} \varepsilon_{12}, \quad \sin^2 \theta_{23} = \frac{1}{2} \frac{(1-\tilde{m}_e)}{(1+\tilde{m}_\mu)} \frac{\tilde{\sigma}_{\ell 2}}{\tilde{m}_\mu} \varepsilon_{23}, \quad \sin^2 \theta_{13} = \frac{1}{2} \frac{\tilde{\sigma}_{\ell 1}}{\tilde{m}_\mu} \varepsilon_{13}, \quad (33)$$

The explicit form of the ε_{ij} parameters is given in the Appendix C 2. From the allowed regions of flavor mixing angles shown in figure 4, we obtain that all charged lepton mass matrices in this equivalent class are able to reproduce the current experimental data of the reactor, solar and atmospheric angles. However of the right panels in figure 5, we

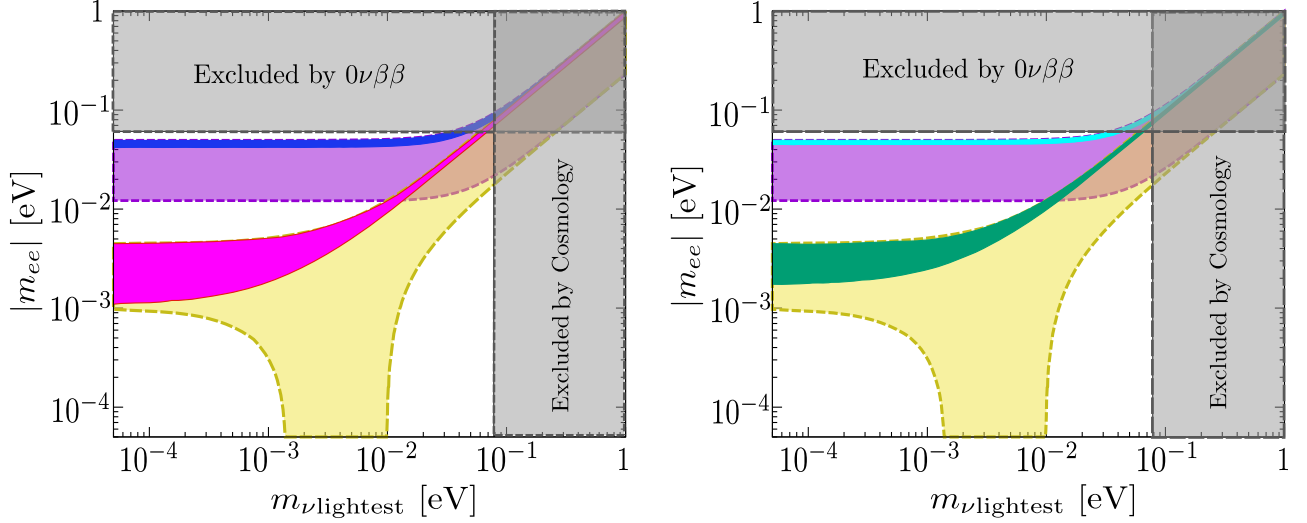


FIG. 6: Plots show the allowed regions for the magnitude of Majorana effective mass $|m_{ee}|$. Respectively, for an inverted and normal neutrino mass hierarchy, the yellow and purple stripes are obtained from the current experimental data on neutrino oscillations at 3σ [5]. In the upper left panel, the magenta area is for a normal hierarchy while the blue area is for an inverted hierarchy, both areas are obtained from \mathbf{M}_ℓ^1 and \mathbf{M}_ℓ^5 . In the upper right panel, the green area is for a normal hierarchy while the cyan area is for an inverted hierarchy, both areas are obtained from \mathbf{M}_ℓ^2 and \mathbf{M}_ℓ^4 . From KamLAND-ZEN [19] and EXO-200 [20] we have the following upper limit $|m_{ee}| < 0.061$, which correspond to the horizontal grey band, whereas vertical grey band corresponds to results reported by Planck collaboration [21].

can conclude that when considering the same numerical values interval for the phase factor ϕ_c , in this equivalent class the mass matrices \mathbf{M}_ℓ^1 , \mathbf{M}_ℓ^2 , \mathbf{M}_ℓ^4 and \mathbf{M}_ℓ^5 are the only ones that can simultaneously reproduce the experimental data of the three mixing angles. Consequently, to reproduce the values for the leptonic flavor mixing angles, at 3σ obtained from the global fit eq. (11), for a normal and inverted hierarchy, the free parameter δ_ℓ should be in the following numerical interval:

$$\begin{aligned} \delta_\ell &\in [1.054, 1.058] \quad \text{for } \mathbf{M}_\ell^1 \text{ and } \mathbf{M}_\ell^5, \\ \delta_\ell &\in [1.0013, 1.0052] \quad \text{for } \mathbf{M}_\ell^2 \text{ and } \mathbf{M}_\ell^4. \end{aligned} \quad (34)$$

In this equivalent class, from expressions in Appendix C 2 and figure 5 we have:

1. For the mass matrices \mathbf{M}_ℓ^1 and \mathbf{M}_ℓ^5 , the reactor, solar and atmospheric mixing angles have a weak dependence on the phase factors ϕ_a . However, the atmospheric and reactor angles have a weak dependence on the phase factor ϕ_c . On the other hand, to reproduce the current experimental data, at 3σ eq.(11), from the right panels in figure 5 for the θ_{12} angle we see that:

$$\begin{aligned} \phi_c &\in [-140^\circ, 140^\circ] \quad \text{for } \mathbf{M}_\ell^1, \\ |\phi_c| &\in [38^\circ, 180^\circ] \quad \text{for } \mathbf{M}_\ell^5. \end{aligned} \quad (35)$$

2. For the mass matrices \mathbf{M}_ℓ^2 and \mathbf{M}_ℓ^4 , the reactor and atmospheric mixing angles do not have an explicit dependence on phase factor ϕ_c . The solar angle has a weak dependence on phase factors ϕ_a and ϕ_c . While the reactor angle

has a weak dependence on phase factor ϕ_a . On the other hand, to reproduce the current experimental data, at 3σ eq.(11), from the right panels in figure 5 for the θ_{23} angle we obtain:

$$|\phi_a| \in [73^\circ, 180^\circ] \text{ for } \mathbf{M}_\ell^2 \text{ and } \mathbf{M}_\ell^4. \quad (36)$$

In figure 6 we show the allowed regions for the magnitude of the Majorana effective mass $|m_{ee}|$, eq. (14), which were obtained in a model-independent context where the neutrino mass matrix has the form given in eq. (9), while the charged lepton matrix is represented for an element of the equivalent class with two texture zeros type-II. eq. (19). Each one of these regions was obtained by considering the values given in eqs. (34)-(36) for the free parameter δ_ℓ and the associated to the CP violation phases ϕ_a and ϕ_c .

C. Equivalent class with two texture zeros type-III

The equivalent class for Hermitian matrices with two texture zeros type-III have the form [18]:

$$\begin{aligned} \mathbf{M}_\ell^0 &= \begin{pmatrix} 0 & a_\ell & e_\ell \\ a_\ell^* & 0 & c_\ell \\ e_\ell^* & c_\ell^* & d_\ell \end{pmatrix}, \quad \mathbf{M}_\ell^1 = \begin{pmatrix} 0 & a_\ell^* & c_\ell \\ a_\ell & 0 & e_\ell \\ c_\ell^* & e_\ell^* & d_\ell \end{pmatrix}, \quad \mathbf{M}_\ell^2 = \begin{pmatrix} d_\ell & c_\ell^* & e_\ell^* \\ c_\ell & 0 & a_\ell^* \\ e_\ell & a_\ell & 0 \end{pmatrix}, \\ \mathbf{M}_\ell^3 &= \begin{pmatrix} 0 & e_\ell & a_\ell \\ e_\ell^* & d_\ell & c_\ell^* \\ a_\ell^* & c_\ell & 0 \end{pmatrix}, \quad \mathbf{M}_\ell^4 = \begin{pmatrix} d_\ell & e_\ell^* & c_\ell^* \\ e_\ell & 0 & a_\ell \\ c_\ell & a_\ell^* & 0 \end{pmatrix}, \quad \mathbf{M}_\ell^5 = \begin{pmatrix} 0 & c_\ell & a_\ell^* \\ c_\ell^* & d_\ell & e_\ell^* \\ a_\ell & e_\ell & 0 \end{pmatrix}, \end{aligned} \quad (37)$$

where

$$\begin{aligned} a_\ell &= \sqrt{\frac{1}{1+\tan^2 \beta_\ell} \frac{\tilde{m}_e \tilde{m}_\mu}{1-\delta_\ell}} e^{i\phi_a}, \quad c_\ell = \left(\frac{1-\tan^2 \beta_\ell}{1+\tan^2 \beta_\ell} \sqrt{\frac{f_{\ell 1} f_{\ell 2} f_{\ell 3}}{1-\delta_\ell}} + [\mathbf{s}_3 - 2(1-\delta_\ell) + \mathbf{s}_1 \tilde{m}_e + \mathbf{s}_2 \tilde{m}_\mu] \frac{\tan \beta_\ell}{1+\tan^2 \beta_\ell} \right) e^{i\phi_c}, \\ e_\ell &= \sqrt{\frac{\tan^2 \beta_\ell}{1+\tan^2 \beta_\ell} \frac{\tilde{m}_e \tilde{m}_\mu}{1-\delta_\ell}} e^{i\phi_e}, \quad d_\ell = \frac{2 \tan \beta_\ell}{1+\tan^2 \beta_\ell} \sqrt{\frac{f_{\ell 1} f_{\ell 2} f_{\ell 3}}{1-\delta_\ell}} + (\mathbf{s}_3 + \mathbf{s}_1 \tilde{m}_e + \mathbf{s}_2 \tilde{m}_\mu) \frac{\tan^2 \beta_\ell}{1+\tan^2 \beta_\ell} + (1-\delta_\ell) \frac{1-\tan^2 \beta_\ell}{1+\tan^2 \beta_\ell}, \\ \tan \beta_{\ell \pm} &= \sqrt{\frac{f_{\ell 1} f_{\ell 2} f_{\ell 3}}{(1-\delta_\ell)^3}} \left(1 \pm \sqrt{1 - \frac{(\mathbf{s}_3 - (1-\delta_\ell) + \mathbf{s}_1 \tilde{m}_e + \mathbf{s}_2 \tilde{m}_\mu)(1-\delta_\ell)^2}{f_{\ell 1} f_{\ell 2} f_{\ell 3}}} \right), \end{aligned} \quad (38)$$

with $f_{\ell 1} = 1 - \mathbf{s}_1 \tilde{m}_e - \delta_\ell$, $f_{\ell 2} = \mathbf{s}_3 (1 - \mathbf{s}_2 \tilde{m}_\mu - \delta_\ell)$, $f_{\ell 3} = 1 + \mathbf{s}_3 (\delta_\ell - 1)$, $\tilde{m}_e = \frac{m_e}{m_\tau}$, $\tilde{m}_\mu = \frac{m_\mu}{m_\tau}$, $\phi_a = \arg \{a_\ell\}$, $\phi_c = \arg \{c_\ell\}$, and $\phi_e = \arg \{e_\ell\}$. In this case, the diagonal matrix of phase factors is $\mathbf{P}_\ell = \text{diag}(1, e^{i\phi_a}, e^{i(\phi_a + \phi_c)})$, while the phase factors satisfy the relation $\phi_e = \phi_a + \phi_c$. The real orthogonal matrix \mathbf{O}_ℓ is constructed with the help of the general eigenvectors given in eq. (B2), which are the eigenvectors of the charged lepton mass matrix. The explicit form of $\mathbf{O}_\ell = (|M_1\rangle, |M_2\rangle, |M_3\rangle)$ is

$$\mathbf{O}_\ell = \mathbf{R}^\top \mathcal{O}_\ell \quad (39)$$

where

$$\mathbf{R} = \begin{pmatrix} 1 & 0 & 0 \\ 0 & \frac{1}{\sqrt{1+\tan^2 \beta_\ell}} & \frac{\tan \beta_\ell}{\sqrt{1+\tan^2 \beta_\ell}} \\ 0 & -\frac{\tan \beta_\ell}{\sqrt{1+\tan^2 \beta_\ell}} & \frac{1}{\sqrt{1+\tan^2 \beta_\ell}} \end{pmatrix} \quad \text{and} \quad \mathcal{O}_\ell = \begin{pmatrix} \mathbf{s}_1 \sqrt{\frac{\tilde{m}_\mu f_{\ell 1}}{D_{\ell 1}}} & \mathbf{s}_2 \sqrt{\frac{\tilde{m}_e f_{\ell 2}}{D_{\ell 2}}} & \mathbf{s}_3 \sqrt{\frac{\tilde{m}_e \tilde{m}_\mu f_{\ell 3}}{D_{\ell 3}}} \\ \sqrt{\frac{\tilde{m}_e (1-\delta_\ell) f_{\ell 1}}{D_{\ell 1}}} & \sqrt{\frac{\tilde{m}_\mu (1-\delta_\ell) f_{\ell 2}}{D_{\ell 2}}} & \sqrt{\frac{(1-\delta_\ell) f_{\ell 3}}{D_{\ell 3}}} \\ -\sqrt{\frac{\tilde{m}_e f_{\ell 2} f_{\ell 3}}{D_{\ell 1}}} & \mathbf{s}_1 \mathbf{s}_2 \sqrt{\frac{\tilde{m}_\mu f_{\ell 1} f_{\ell 3}}{D_{\ell 2}}} & \mathbf{s}_3 \sqrt{\frac{f_{\ell 1} f_{\ell 2}}{D_{\ell 3}}} \end{pmatrix}, \quad (40)$$

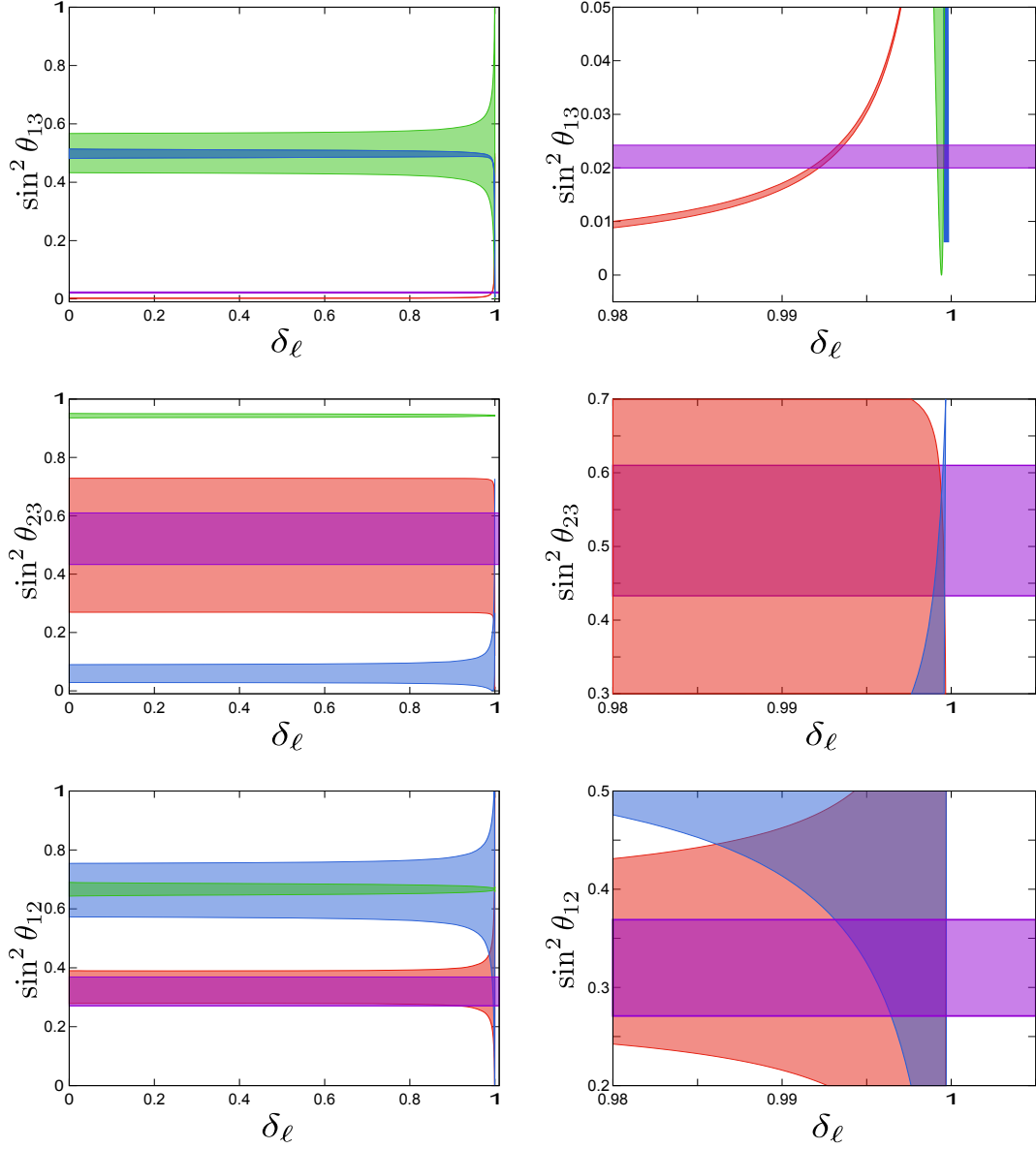


FIG. 7: The allowed regions for the reactor (upper panels), atmospheric (middle panels), and solar (lower panels) mixing angles and free parameter δ_ℓ . The purple stripe corresponds to the values at 3σ for the reactor, atmospheric and solar mixing angles obtained from the global fit, for normal and inverted hierarchy [5]. In these panels, the red area is for \mathbf{M}_ℓ^0 and \mathbf{M}_ℓ^3 , blue area is for \mathbf{M}_ℓ^1 and \mathbf{M}_ℓ^5 , the green area is for \mathbf{M}_ℓ^2 and \mathbf{M}_ℓ^4 . The right panels show a zoom-in of the region where the theoretical expressions for the mixing angles simultaneously reproduce the current experimental data.

with

$$\begin{aligned}
 D_{\ell 1} &= (1 - \delta_\ell) (\tilde{m}_\mu + \mathbf{s}_3 \tilde{m}_e) (1 + \mathbf{s}_2 \tilde{m}_e), & D_{\ell 2} &= (1 - \delta_\ell) (\tilde{m}_\mu + \mathbf{s}_3 \tilde{m}_e) (1 + \mathbf{s}_1 \tilde{m}_\mu), \\
 D_{\ell 3} &= (1 - \delta_\ell) (1 + \mathbf{s}_2 \tilde{m}_e) (1 + \mathbf{s}_1 \tilde{m}_\mu).
 \end{aligned}
 \tag{41}$$

The parameter δ_ℓ must satisfy the conditions

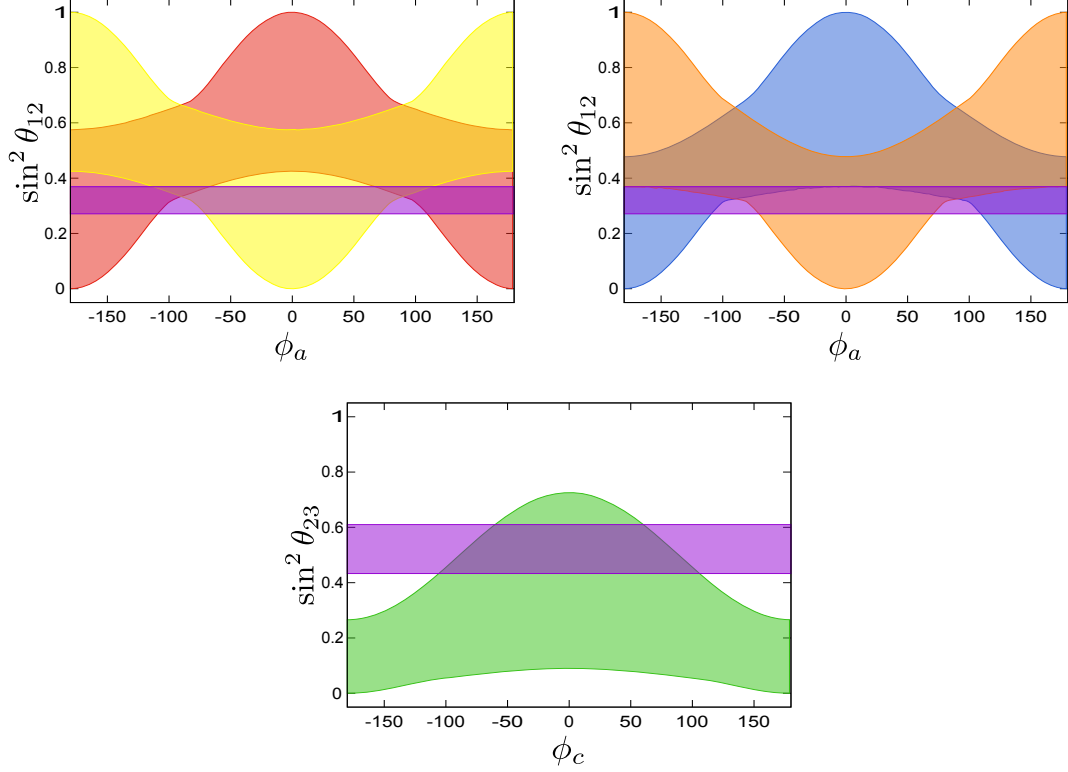


FIG. 8: The allowed regions for the solar (upper panels) and atmospheric (lower panel) mixing angles and free parameters ϕ_a and ϕ_c . The purple stripe corresponds to the values at 3σ for the solar and atmospheric mixing angles obtained from the global fit, for normal and inverted hierarchy [5]. In the upper panels, the red area is for \mathbf{M}_ℓ^0 , yellow area is for \mathbf{M}_ℓ^3 , blue area is for \mathbf{M}_ℓ^1 , orange area is for \mathbf{M}_ℓ^5 . In the lower panel, the green area is for \mathbf{M}_ℓ^0 and \mathbf{M}_ℓ^3 .

$$\begin{aligned}
 \text{A. } & 0 < \delta_\ell < 1 - \tilde{m}_\mu, & \text{for } & m_e = -m_e \quad (\mathbf{s}_1 = -1, \mathbf{s}_2 = +1, \mathbf{s}_3 = +1). \\
 \text{B. } & 0 < \delta_\ell < 1 - \tilde{m}_e, \quad \delta_\ell \neq \tilde{m}_\mu - \tilde{m}_e, & \text{for } & m_\mu = -m_\mu \quad (\mathbf{s}_1 = +1, \mathbf{s}_2 = -1, \mathbf{s}_3 = +1). \\
 \text{C. } & 1 - \tilde{m}_\mu < \delta_\ell < 1 - \tilde{m}_e, & \text{for } & m_\tau = -m_\tau \quad (\mathbf{s}_1 = +1, \mathbf{s}_2 = +1, \mathbf{s}_3 = -1).
 \end{aligned} \tag{42}$$

In this case, the flavor mixing angles in eq. (6) have the form:

$$\sin^2 \theta_{12} = \frac{1}{3} \frac{\tilde{m}_e}{\tilde{m}_\mu} \varepsilon_{12}, \quad \sin^2 \theta_{23} = \frac{1}{2} \frac{(1 + \mathbf{s}_2 \tilde{m}_e)}{(1 + \mathbf{s}_1 \tilde{m}_\mu)} \varepsilon_{23}, \quad \sin^2 \theta_{13} = \frac{1}{2} \frac{\tilde{m}_e}{\tilde{m}_\mu} \varepsilon_{13}. \tag{43}$$

The explicit form of the ε_{ij} parameters is given in the Appendix C 3. From the allowed regions of flavor mixing angles shown in figure 7, and computed taken into account the condition **B** (42) and for $\tan \beta_{\ell+}$ (38), we obtain that in this equivalent class, the charged lepton mass matrices \mathbf{M}_ℓ^2 and \mathbf{M}_ℓ^4 cannot correctly reproduce current experimental data of the solar and atmospheric mixing angles. So to reproduce the values for the leptonic flavor mixing angles, at 3σ obtained from the global fit eq. (11), for a normal and inverted hierarchy, the free parameter δ_ℓ should be in the following numerical interval:

$$\begin{aligned}
 \delta_\ell & \in [0.9916, 0.9936] \quad \text{for } \mathbf{M}_\ell^0 \text{ and } \mathbf{M}_\ell^3, \\
 \delta_\ell & \approx 0.9997 \quad \text{for } \mathbf{M}_\ell^1 \text{ and } \mathbf{M}_\ell^5.
 \end{aligned} \tag{44}$$

In this equivalent class, from expressions in Appendix C 3 and figure 8 we have:

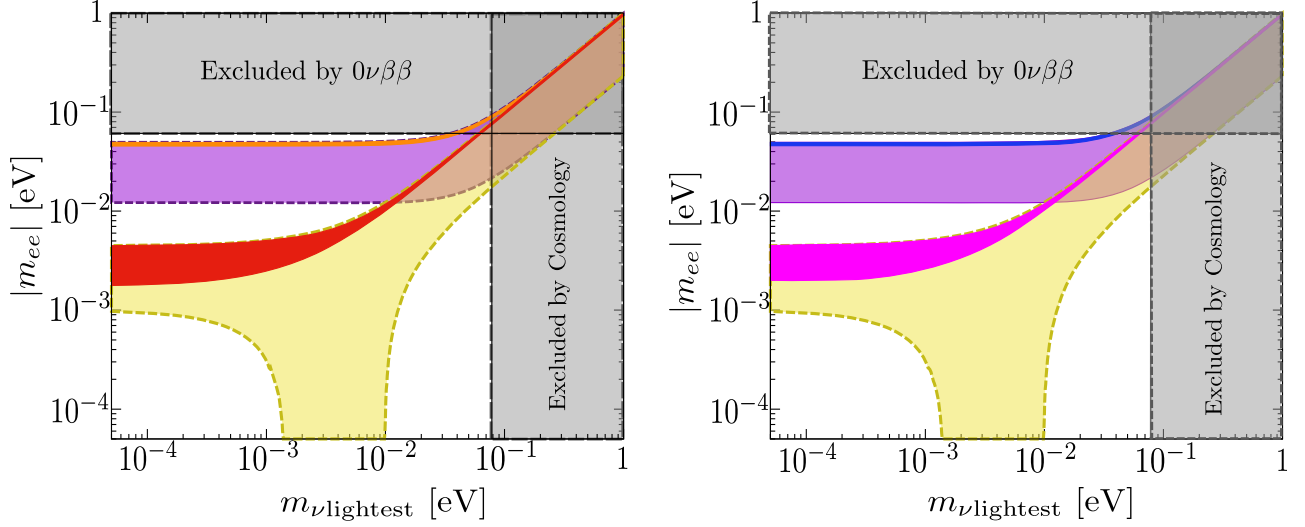


FIG. 9: These panels show the allowed regions for the magnitude of Majorana effective mass $|m_{ee}|$. Respectively, for an inverted and normal neutrino mass hierarchy, the yellow and purple stripes are obtained from the current experimental data on neutrino oscillations at 3σ [5]. In the upper right panel, the magenta area is for a normal hierarchy while the blue area is for an inverted hierarchy, both areas are obtained from \mathbf{M}_ℓ^1 and \mathbf{M}_ℓ^5 . In the upper left panel, the red area is for a normal hierarchy while the orange area is for an inverted hierarchy, both areas are obtained from \mathbf{M}_ℓ^2 and \mathbf{M}_ℓ^4 . From KamLAND-ZEN [19] and EXO-200 [20] we have the following upper limit $|m_{ee}| < 0.061$, which correspond to the horizontal grey band, whereas vertical grey band corresponds to results reported by Planck collaboration [21].

1. For the mass matrices \mathbf{M}_ℓ^0 and \mathbf{M}_ℓ^3 , the reactor and atmospheric mixing angles do not have an explicit dependence on phase factor ϕ_a . While the solar and reactor mixing angles have a weak dependence on phase factors ϕ_c . On the other hand, to reproduce the current experimental data, at 3σ eq.(11), from the upper left and lower panels in figure 8 for the θ_{12} and θ_{23} angles we obtain that:

$$\begin{aligned}
 |\phi_a| &\in [67^\circ, 180^\circ] \quad \text{for } \mathbf{M}_\ell^0, \\
 \phi_a &\in [-113^\circ, 113^\circ] \quad \text{for } \mathbf{M}_\ell^3, \\
 \phi_c &\in [-106^\circ, 106^\circ] \quad \text{for } \mathbf{M}_\ell^0 \text{ and } \mathbf{M}_\ell^3.
 \end{aligned} \tag{45}$$

2. For the mass matrices \mathbf{M}_ℓ^1 and \mathbf{M}_ℓ^5 , the reactor and atmospheric mixing angles have a weak dependence on phase factors ϕ_a and ϕ_c . While the solar mixing angle has a weak dependence on phase factor ϕ_c . On the other hand, to reproduce the current experimental data, at 3σ eq.(11), from the upper right panel in figure 8 for the θ_{12} angle we obtain that:

$$\begin{aligned}
 |\phi_a| &\in [10^\circ, 180^\circ] \quad \text{for } \mathbf{M}_\ell^1, \\
 \phi_a &\in [-170^\circ, 170^\circ] \quad \text{for } \mathbf{M}_\ell^5.
 \end{aligned} \tag{46}$$

In figure 9 we show the allowed regions for the magnitude of the Majorana effective mass $|m_{ee}|$, ec. (14), which were obtained in a model-independent context where the neutrino mass matrix has the form given in eq. (9), while the

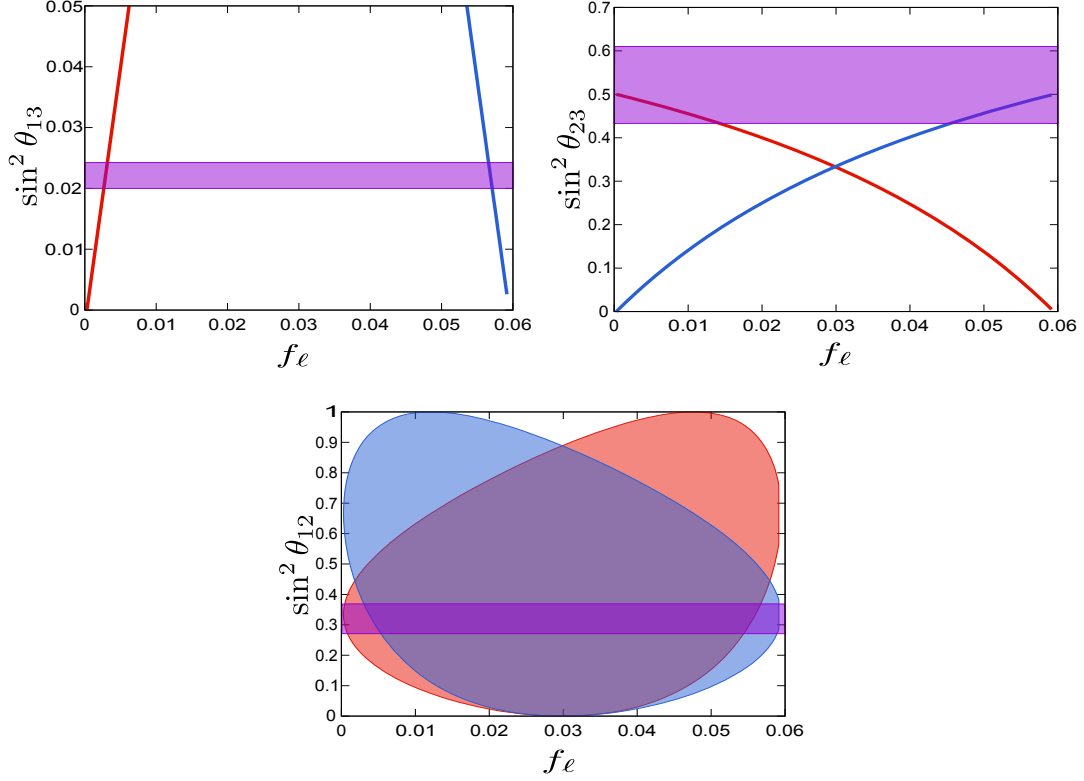


FIG. 10: The allowed regions for the reactor, atmospheric (upper panels), and solar (lower panels) mixing angles and free parameter f_ℓ . The purple stripe corresponds to the values at 3σ for the reactor, atmospheric and solar mixing angles obtained from the global fit, for normal and inverted hierarchy [5]. In these panels, the red area is for \mathbf{M}_ℓ^0 and \mathbf{M}_ℓ^3 , and blue area is for \mathbf{M}_ℓ^1 and \mathbf{M}_ℓ^5 .

charged lepton matrix is represented for an element of the equivalent class with two texture zeros type-III. eq. (37). Each one of these regions was obtained by considering the values given in eqs. (44)-(46) for the free parameter δ_ℓ and the associated to the CP violation phases ϕ_a and ϕ_c .

D. Equivalent class with two texture zeros type-IV

The equivalent class for Hermitian matrices with two texture zeros type-IV have the form [18]:

$$\begin{aligned} \mathbf{M}_\ell^0 &= \begin{pmatrix} f_\ell & a_\ell & 0 \\ a_\ell^* & b_\ell & 0 \\ 0 & 0 & d_\ell \end{pmatrix}, \quad \mathbf{M}_\ell^1 = \begin{pmatrix} b_\ell & a_\ell & 0 \\ a_\ell^* & f_\ell & 0 \\ 0 & 0 & d_\ell \end{pmatrix}, \quad \mathbf{M}_\ell^2 = \begin{pmatrix} d_\ell & 0 & 0 \\ 0 & b_\ell & a_\ell^* \\ 0 & a_\ell & f_\ell \end{pmatrix}, \\ \mathbf{M}_\ell^3 &= \begin{pmatrix} f_\ell & 0 & a_\ell \\ 0 & d_\ell & 0 \\ a_\ell^* & 0 & b_\ell \end{pmatrix}, \quad \mathbf{M}_\ell^4 = \begin{pmatrix} d_\ell & 0 & 0 \\ 0 & f_\ell & a_\ell \\ 0 & a_\ell^* & b_\ell \end{pmatrix}, \quad \mathbf{M}_\ell^5 = \begin{pmatrix} b_\ell & 0 & a_\ell^* \\ 0 & d_\ell & 0 \\ a_\ell & 0 & f_\ell \end{pmatrix}, \end{aligned} \quad (47)$$

where $d_\ell = 1$

$$a_\ell = \sqrt{(f_\ell - \tilde{m}_e)(\tilde{m}_\mu - f_\ell)} e^{i\phi_a}, \quad b_\ell = \tilde{m}_e + \tilde{m}_\mu - f_\ell, \quad (48)$$

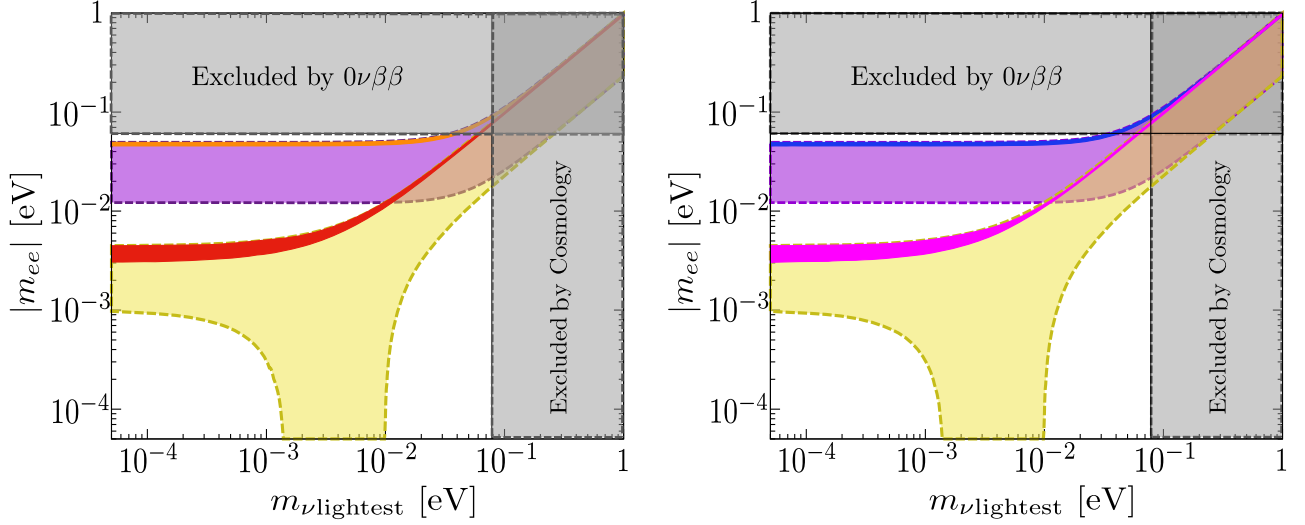


FIG. 11: In these panels, we show the allowed regions for the magnitude of Majorana effective mass $|m_{ee}|$. Respectively, for an inverted and normal neutrino mass hierarchy, the yellow and purple stripes are obtained from the current experimental data on neutrino oscillations at 3σ [5]. In the upper right panel, the magenta area is for a normal hierarchy while the blue area is for an inverted hierarchy, both areas are obtained from \mathbf{M}_ℓ^1 and \mathbf{M}_ℓ^5 . In the upper left panel, the red area is for a normal hierarchy while the orange area is for an inverted hierarchy, both areas are obtained from \mathbf{M}_ℓ^2 and \mathbf{M}_ℓ^4 . From KamLAND-ZEN [19] and EXO-200 [20] we have the following upper limit $|m_{ee}| < 0.061$, which correspond to the horizontal grey band, whereas vertical grey band corresponds to results reported by Planck collaboration [21].

where $\tilde{m}_e = \frac{m_e}{m_\tau}$, $\tilde{m}_\mu = \frac{m_\mu}{m_\tau}$, $\tilde{f}_\ell = \frac{f_\ell}{m_\tau}$, and $\phi_a = \arg\{a_\ell\}$. In this case, the diagonal matrix of phase factors is $\mathbf{P}_\ell = \text{diag}(1, e^{i\phi_a}, e^{i\phi_a})$. The real orthogonal matrix \mathbf{O}_ℓ is

$$\mathbf{O}_\ell = \begin{pmatrix} \sqrt{\frac{\tilde{m}_\mu - \tilde{f}_\ell}{\tilde{m}_\mu - \tilde{m}_e}} & \sqrt{\frac{\tilde{f}_\ell - \tilde{m}_e}{\tilde{m}_\mu - \tilde{m}_e}} & 0 \\ -\sqrt{\frac{\tilde{f}_\ell - \tilde{m}_e}{\tilde{m}_\mu - \tilde{m}_e}} & \sqrt{\frac{\tilde{m}_\mu - \tilde{f}_\ell}{\tilde{m}_\mu - \tilde{m}_e}} & 0 \\ 0 & 0 & 1 \end{pmatrix}. \quad (49)$$

The parameter \tilde{f}_ℓ must satisfy the condition $\tilde{m}_\mu > \tilde{f}_\ell > \tilde{m}_e$. In this case, the flavor mixing angles in eq. (6) have the form:

$$\sin^2 \theta_{12} = \frac{1}{3} \varepsilon_{12}, \quad \sin^2 \theta_{23} = \frac{1}{2} \varepsilon_{23}, \quad \sin^2 \theta_{13} = \frac{1}{2} \frac{\tilde{m}_e}{\tilde{m}_\mu} \varepsilon_{13}. \quad (50)$$

The explicit form of the ε_{ij} parameters is given in the Appendix C4. In this equivalent class, the charged lepton mass matrices \mathbf{M}_ℓ^2 and \mathbf{M}_ℓ^4 cannot correctly reproduce current experimental data of the solar and atmospheric mixing angles, since these mass matrices generate the same theoretical expression for $\varepsilon_{12} = \varepsilon_{23}$. In figure 10 we show the allowed regions for the reactor, atmospheric, and solar mixing angles and the free parameter f_ℓ . From this regions we obtain that to reproduce the values for the leptonic flavor mixing angles, at 3σ , obtained from the global fit, for a

normal and inveterted hierarchy, the free parameter f_ℓ should be in the following numerical interval

$$\begin{aligned} f_\ell &\in [2.66 \times 10^{-3}, 3.16 \times 10^{-3}] && \text{for } \mathbf{M}_\ell^0 \text{ and } \mathbf{M}_\ell^3. \\ f_\ell &\in [5.66 \times 10^{-2}, 5.71 \times 10^{-2}] && \text{for } \mathbf{M}_\ell^1 \text{ and } \mathbf{M}_\ell^5. \end{aligned} \quad (51)$$

For the mass matrices \mathbf{M}_ℓ^0 , \mathbf{M}_ℓ^1 , \mathbf{M}_ℓ^3 and \mathbf{M}_ℓ^5 , the theoretical expressions for reactor and atmospheric mixing angles do not explicitly have a dependence on the phase factor ϕ_a , while the solar angle has a weak dependence on the same phase factor.

In figure 11 we show the allowed regions for the magnitude of the Majorana effective mass $|m_{ee}|$, eq. (14), which were obtained in a model-independent context where the neutrino mass matrix has the form given in eq. (9), while the charged lepton matrix is represented for an element of the equivalent class with two texture zeros type-IV, eq. (47). Each one of these regions was obtained by considering the values given in eqs. (51) for the free parameter f_ℓ .

IV. SUMMARY

In a model-independent theoretical framework, we present a generalization of TBM leptonic flavor mixing pattern. In this modification to the TBM pattern, the unitary matrix that diagonalizes to the neutrino mass matrix is represented by means of TBM flavor mixing pattern, eq. (8), whereas the charged lepton mass matrix is represented by one of the elements of the equivalence classes with two texture zeros, eqs. (19), (28), (37), and (47). For these four equivalent classes, we show a deviation from the TBM pattern in terms of the charged lepton masses as well as the theoretical expressions and their parameter space for the mixing angles. Furthermore, from the theoretical expressions of ε_{ij} in Appendix C we have for each type of equivalent class the \mathbf{M}_ℓ^0 and \mathbf{M}_ℓ^3 matrices generate the same expressions for ϵ_{23} and ϵ_{13} ; similarly for \mathbf{M}_ℓ^2 and \mathbf{M}_ℓ^4 , as well as \mathbf{M}_ℓ^1 and \mathbf{M}_ℓ^5 . Finally, we present the phenomenological implications of numerical values of the “Majorana-like” phase factors on the neutrinoless double-beta decay.

From the analysis performed for the four types of equivalence classes, we had that: For the equivalent class type-I, on the one hand, it is easy to conclude that all charged lepton mass matrices \mathbf{M}_ℓ^i ($i = 0, \dots, 5$) are able to reproduce the current experimental values of reactor, solar and atmospheric angles. But, the numerical interval of the free parameter δ_ℓ , for the \mathbf{M}_ℓ^1 , \mathbf{M}_ℓ^2 , \mathbf{M}_ℓ^4 and \mathbf{M}_ℓ^5 , is too small eq. (25). On the other hand, for all mass matrices \mathbf{M}_ℓ^i ($i = 0, \dots, 5$), the solar and reactor mixing angles have a weak dependence on phases ϕ_a and ϕ_c ; whereas for \mathbf{M}_ℓ^1 and \mathbf{M}_ℓ^5 , the atmospheric mixing angle has a weak dependence on ϕ_a and ϕ_c . However, to reproduce the current experimental data for the mixing angle θ_{23} , eq. (11), for \mathbf{M}_ℓ^0 and \mathbf{M}_ℓ^3 , the phase ϕ_c is in the numerical interval (26); for \mathbf{M}_ℓ^2 and \mathbf{M}_ℓ^4 , ϕ_a runs over the numerical interval (27).

In case of the equivalent class type-II, the charged lepton mass matrices \mathbf{M}_ℓ^0 and \mathbf{M}_ℓ^3 cannot simultaneously reproduce the current experimental data on the neutrino oscillations. But the remaining mass matrices, \mathbf{M}_ℓ^1 , \mathbf{M}_ℓ^2 , \mathbf{M}_ℓ^4 and \mathbf{M}_ℓ^5 , reproduce the experimental values of the three leptonic mixing angles, where the free parameter δ_ℓ has the numerical interval given in eq. (34). Moreover, for these four mass matrices, the reactor mixing angle has a weak dependence on the phases ϕ_a and ϕ_c . The solar mixing angle has a weak dependence on the phases ϕ_a and ϕ_c for the \mathbf{M}_ℓ^2 and \mathbf{M}_ℓ^4 , whereas to reproduce the current experimental data for θ_{12} , eq. (11); for \mathbf{M}_ℓ^1 and \mathbf{M}_ℓ^5 , the phase ϕ_c is in the numerical interval given in eq. (35). The atmospheric mixing angle has a weak dependence on the phases ϕ_a and ϕ_c for the \mathbf{M}_ℓ^1 and \mathbf{M}_ℓ^5 . Nevertheless, to reproduce the current experimental data for θ_{23} , for \mathbf{M}_ℓ^2 and \mathbf{M}_ℓ^4 , the

phase ϕ_a run over numerical interval given in eq. (36).

For the equivalent class type-III, the charged lepton mass matrices \mathbf{M}_ℓ^2 and \mathbf{M}_ℓ^4 cannot simultaneously reproduce the current experimental data on the neutrino oscillations. However, for the numerical interval of the free parameter δ_ℓ given in eq. (44), \mathbf{M}_ℓ^0 , \mathbf{M}_ℓ^1 , \mathbf{M}_ℓ^3 and \mathbf{M}_ℓ^5 , correctly reproduce the experimental data of the three leptonic mixing angles. For the four previous matrices, the reactor mixing angle has a weak dependence on phases ϕ_a and ϕ_c . The atmospheric mixing angle has a weak dependence on the phases ϕ_a and ϕ_c for the \mathbf{M}_ℓ^2 and \mathbf{M}_ℓ^4 , while to reproduce the experimental data for θ_{23} , for \mathbf{M}_ℓ^1 and \mathbf{M}_ℓ^5 , the phase ϕ_a is in the numerical interval given in eq. (45). Furthermore, to reproduce the current experimental data for the solar mixing angle for the four charged lepton mass matrices, the phase factors ϕ_a and ϕ_c are in the numerical intervals given in eqs. (45) and (46).

Finally, of the equivalent class type-IV we concluded that the charged lepton mass matrices \mathbf{M}_ℓ^2 and \mathbf{M}_ℓ^4 cannot simultaneously reproduce the current experimental data on the neutrino oscillations, since for these mass matrices $\varepsilon_{12} = \varepsilon_{23}$. However, the remaining four mass matrices reproduce the experimental data of the three lepton mixing angles, where the numerical interval of the free parameter f_ℓ is given in eq. (51). And for this case, the atmospheric, reactor, and solar mixing angles have a weak dependence on phase factor ϕ_a .

Appendix A: Permutation group

The permutations of symmetry group S_3 can be represented on the reducible triplet as [22, 23]:

$$\begin{aligned} \mathbf{T}_0 &= \begin{pmatrix} 1 & 0 & 0 \\ 0 & 1 & 0 \\ 0 & 0 & 1 \end{pmatrix}, \quad \mathbf{T}_1 = \begin{pmatrix} 0 & 1 & 0 \\ 1 & 0 & 0 \\ 0 & 0 & 1 \end{pmatrix}, \quad \mathbf{T}_2 = \begin{pmatrix} 0 & 0 & 1 \\ 0 & 1 & 0 \\ 1 & 0 & 0 \end{pmatrix}, \\ \mathbf{T}_3 &= \begin{pmatrix} 1 & 0 & 0 \\ 0 & 0 & 1 \\ 0 & 1 & 0 \end{pmatrix}, \quad \mathbf{T}_4 = \begin{pmatrix} 0 & 1 & 0 \\ 0 & 0 & 1 \\ 1 & 0 & 0 \end{pmatrix}, \quad \mathbf{T}_5 = \begin{pmatrix} 0 & 0 & 1 \\ 1 & 0 & 0 \\ 0 & 1 & 0 \end{pmatrix}. \end{aligned} \tag{A1}$$

Appendix B: General Eigenvector for a 3×3 complex matrix

The general shape of a 3×3 matrix is:

$$\mathbf{M} = \begin{pmatrix} m_{11} & m_{12} & m_{13} \\ m_{21} & m_{22} & m_{23} \\ m_{31} & m_{32} & m_{33} \end{pmatrix}, \tag{B1}$$

where all elements of \mathbf{M} are complex. The three eigenvalues, $|\mathbf{M}_k\rangle$, of the \mathbf{M} matrix have the form [24]:

$$|M_k\rangle = \frac{1}{N_k} \begin{pmatrix} a_k \\ b_k \\ c_k \end{pmatrix} = \frac{1}{N_k} \begin{pmatrix} (\lambda_k - m_{22})m_{13} + m_{12}m_{23} \\ (\lambda_k - m_{11})m_{23} + m_{21}m_{13} \\ (\lambda_k - m_{11})(\lambda_k - m_{22}) - m_{12}m_{21} \end{pmatrix}. \tag{B2}$$

In this expression the λ_k , with $k = 1, 2, 3$, correspond to the eigenvalues of the \mathbf{M} matrix, and the $N_k \equiv \sqrt{\langle \mathbf{M}_k | \mathbf{M}_k \rangle}$ are the normalization constants. Now, it is easy to show that the $|\mathbf{M}_k\rangle$ are the eigenvectors of the \mathbf{M} matrix, we only

need to consider the eigenvalues equation $\mathbf{M} |\mathbf{M}_k\rangle = \lambda_k |\mathbf{M}_k\rangle$ and the explicit form of the characteristic polynomial which is given by the expression $\det \{\lambda_k \mathbb{I}_{3 \times 3} - \mathbf{M}\} = 0$. The explicit form of the eigenvalues equation is

$$\begin{pmatrix} m_{11} & m_{12} & m_{13} \\ m_{21} & m_{22} & m_{23} \\ m_{31} & m_{32} & m_{33} \end{pmatrix} \begin{pmatrix} a_k \\ b_k \\ c_k \end{pmatrix} = \lambda_k \begin{pmatrix} a_k \\ b_k \\ c_k \end{pmatrix}. \quad (\text{B3})$$

The first row of the right-handed side of eq. (B3) is

$$\begin{aligned} m_{11}a_k + m_{12}b_k + m_{13}c_k &= m_{11}((\lambda_k - m_{22})m_{13} + m_{12}m_{23}) + m_{12}((\lambda_k - m_{11})m_{23} + m_{21}m_{13}) \\ &\quad + m_{13}((\lambda_k - m_{11})(\lambda_k - m_{22}) - m_{12}m_{21}), \\ &= \lambda_k((\lambda_k - m_{22})m_{13} + m_{12}m_{23}), \\ &= \lambda_k a_k. \end{aligned} \quad (\text{B4})$$

The second row of the right-handed side of eq. (B3) is

$$\begin{aligned} m_{21}a_k + m_{22}b_k + m_{23}c_k &= m_{21}((\lambda_k - m_{22})m_{13} + m_{12}m_{23}) + m_{22}((\lambda_k - m_{11})m_{23} + m_{21}m_{13}) \\ &\quad + m_{23}((\lambda_k - m_{11})(\lambda_k - m_{22}) - m_{12}m_{21}), \\ &= \lambda_k((\lambda_k - m_{11})m_{23} + m_{21}m_{13}), \\ &= \lambda_k b_k. \end{aligned} \quad (\text{B5})$$

The third row of the right-handed side of eq. (B3) is

$$\begin{aligned} m_{31}a_k + m_{32}b_k + m_{33}c_k &= m_{31}((\lambda_k - m_{22})m_{13} + m_{12}m_{23}) + m_{32}((\lambda_k - m_{11})m_{23} + m_{21}m_{13}) \\ &\quad + m_{33}((\lambda_k - m_{11})(\lambda_k - m_{22}) - m_{12}m_{21}), \\ &= (\lambda_k - m_{22})m_{13}m_{31} + m_{31}m_{12}m_{23} + m_{32}m_{21}m_{13} + (\lambda_k - m_{11})m_{32}m_{23} \\ &\quad + (\lambda_k - m_{22})(\lambda_k - m_{11})m_{33} - m_{33}m_{12}m_{21}. \end{aligned} \quad (\text{B6})$$

With help of the characteristic polynomial in terms of \mathbf{M} matrix invariants (trace and determinant) [24]

$$\lambda_i^3 - \text{Tr}\{\mathbf{M}\}\lambda_i^2 - \chi\{\mathbf{M}\}\lambda_i - \det\{\mathbf{M}\} = 0, \quad (\text{B7})$$

where $\chi\{\mathbf{M}\}$ is a function of the trace with the following explicit form:

$$\chi\{\mathbf{M}\} \equiv -\text{Tr}\{\text{adj}\{\mathbf{M}\}\} = \frac{1}{2} \left(\text{Tr}\{\mathbf{M}^2\} - \text{Tr}\{\mathbf{M}\}^2 \right). \quad (\text{B8})$$

We obtain that

$$\begin{aligned} (\lambda_k - m_{22})m_{13}m_{31} + m_{31}m_{12}m_{23} + m_{32}m_{21}m_{13} + (\lambda_k - m_{11})m_{32}m_{23} + (\lambda_k - m_{22})(\lambda_k - m_{11})m_{33} \\ - m_{33}m_{12}m_{21} = \lambda_k((\lambda_k - m_{11})(\lambda_k - m_{22}) - m_{12}m_{21}) = \lambda_k c_k. \end{aligned} \quad (\text{B9})$$

From eq. (B9) the expression in eq. (B6) takes the form:

$$m_{31}a_k + m_{32}b_k + m_{33}c_k = \lambda_k((\lambda_k - m_{11})(\lambda_k - m_{22}) - m_{12}m_{21}) = \lambda_k c_k. \quad (\text{B10})$$

Now, with help of Eqs. (B4), (B5) and (B10) we can conclude that the vectors $|\mathbf{M}_k\rangle$ are eigenvectors of \mathbf{M} matrix.

Appendix C: Mixing angles parameters

1. Parameters of equivalent class with two texture zeros type-I

For the mass matrices \mathbf{M}_ℓ^0 and \mathbf{M}_ℓ^3 ,

$$\begin{aligned}\varepsilon_{23} &= \frac{(1+s_3(\delta_\ell-1))f_{\ell 1}+(1-\delta_\ell)f_{\ell 2}+s_1s_22\sqrt{(1+s_3(\delta_\ell-1))(1-\delta_\ell)f_{\ell 1}f_{\ell 2}\cos\phi_c}}{(1-\delta_\ell)\left(1+s_3\frac{\tilde{m}_e}{\tilde{m}_\mu}\right)(1+s_2\tilde{m}_e)+\frac{1}{2}\frac{\tilde{m}_e}{\tilde{m}_\mu}\left(f_{\ell 2}(1+s_3(\delta_\ell-1))+f_{\ell 1}(1-\delta_\ell)-2\sqrt{(1+s_3(\delta_\ell-1))(1-\delta_\ell)f_{\ell 1}f_{\ell 2}\cos\phi_c}\right)}, \\ \varepsilon_{13} &= \frac{f_{\ell 2}(1+s_3(\delta_\ell-1))+f_{\ell 1}(1-\delta_\ell)-2\sqrt{(1-\delta_\ell)(1+s_3(\delta_\ell-1))f_{\ell 1}f_{\ell 2}\cos\phi_c}}{(1-\delta_\ell)\left(1+s_3\frac{\tilde{m}_e}{\tilde{m}_\mu}\right)(1+s_2\tilde{m}_e)}, \\ \varepsilon_{12} &= \frac{f_{\ell 2}(1+s_3(\delta_\ell-1))+f_{\ell 1}\frac{\tilde{m}_\mu}{\tilde{m}_e}+f_{\ell 1}(1-\delta_\ell)+2\sqrt{(1+s_3(\delta_\ell-1))(1-\delta_\ell)f_{\ell 1}f_{\ell 2}c_c}+(-1)^i s_1 2\left(\sqrt{\frac{\tilde{m}_\mu}{\tilde{m}_e}(1+s_3(\delta_\ell-1))f_{\ell 1}f_{\ell 2}c_{ac}}+f_{\ell 1}\sqrt{\frac{\tilde{m}_\mu}{\tilde{m}_e}(1-\delta_\ell)c_a}\right)}{(1-\delta_\ell)\left(1+s_3\frac{\tilde{m}_e}{\tilde{m}_\mu}\right)(1+s_2\tilde{m}_e)-\frac{1}{2}\frac{\tilde{m}_e}{\tilde{m}_\mu}f_{\ell 2}(1+s_3(\delta_\ell-1))+(1-\delta_\ell)f_{\ell 1}-2\sqrt{(1-\delta_\ell)(1+s_3(\delta_\ell-1))f_{\ell 1}f_{\ell 2}c_c}},\end{aligned}\tag{C1}$$

where $i = 0$ for \mathbf{M}_ℓ^0 , $i = 1$ for \mathbf{M}_ℓ^3 , $c_a = \cos\phi_a$, $c_c = \cos\phi_c$, and $c_{ac} = \cos(\phi_a + \phi_c)$. For \mathbf{M}_ℓ^1 and \mathbf{M}_ℓ^5

$$\begin{aligned}\varepsilon_{23} &= \frac{\frac{\tilde{m}_e}{\tilde{m}_\mu}f_{\ell 2}+(1+s_3(\delta_\ell-1))f_{\ell 1}+s_12\sqrt{\frac{\tilde{m}_e}{\tilde{m}_\mu}(1+s_3(\delta_\ell-1))f_{\ell 1}f_{\ell 2}\cos(\phi_a+\phi_c)}}{(1-\delta_\ell)\left(1+s_3\frac{\tilde{m}_e}{\tilde{m}_\mu}\right)(1+s_2\tilde{m}_e)-\frac{1}{2}\frac{\tilde{m}_e}{\tilde{m}_\mu}\left(f_{\ell 2}(1+s_3(\delta_\ell-1))+\frac{\tilde{m}_\mu}{\tilde{m}_e}f_{\ell 1}-s_12\sqrt{\frac{\tilde{m}_\mu}{\tilde{m}_e}(1+s_3(\delta_\ell-1))f_{\ell 1}f_{\ell 2}\cos(\phi_a+\phi_c)}\right)}, \\ \varepsilon_{13} &= \frac{f_{\ell 2}(1+s_3(\delta_\ell-1))+\frac{\tilde{m}_\mu}{\tilde{m}_e}f_{\ell 1}-s_12\sqrt{\frac{\tilde{m}_\mu}{\tilde{m}_e}(1+s_3(\delta_\ell-1))f_{\ell 1}f_{\ell 2}\cos(\phi_a+\phi_c)}}{(1-\delta_\ell)\left(1+s_3\frac{\tilde{m}_e}{\tilde{m}_\mu}\right)(1+s_2\tilde{m}_e)}, \\ \varepsilon_{12} &= \frac{f_{\ell 2}(1+s_3(\delta_\ell-1))+f_{\ell 1}\frac{\tilde{m}_\mu}{\tilde{m}_e}+f_{\ell 1}(1-\delta_\ell)+2s_1\sqrt{\frac{\tilde{m}_\mu}{\tilde{m}_e}(1+s_3(\delta_\ell-1))f_{\ell 1}f_{\ell 2}c_{ac}}+(-1)^i 2\left(\sqrt{(1+s_3(\delta_\ell-1))(1-\delta_\ell)f_{\ell 1}f_{\ell 2}c_c}+s_1f_{\ell 1}\sqrt{\frac{\tilde{m}_\mu}{\tilde{m}_e}(1-\delta_\ell)c_a}\right)}{(1-\delta_\ell)\left(1+s_3\frac{\tilde{m}_e}{\tilde{m}_\mu}\right)(1+s_2\tilde{m}_e)-\frac{1}{2}\frac{\tilde{m}_e}{\tilde{m}_\mu}f_{\ell 2}(1+s_3(\delta_\ell-1))+f_{\ell 1}\frac{\tilde{m}_\mu}{\tilde{m}_e}-2s_1\sqrt{\frac{\tilde{m}_\mu}{\tilde{m}_e}(1+s_3(\delta_\ell-1))f_{\ell 1}f_{\ell 2}c_{ac}}},\end{aligned}\tag{C2}$$

where $i = 0$ for \mathbf{M}_ℓ^1 , $i = 1$ for \mathbf{M}_ℓ^5 , $c_a = \cos\phi_a$, $c_c = \cos\phi_c$, and $c_{ac} = \cos(\phi_a + \phi_c)$. For \mathbf{M}_ℓ^2 and \mathbf{M}_ℓ^4

$$\begin{aligned}\varepsilon_{23} &= \frac{f_{\ell 2}\left(1-\delta_\ell+\frac{\tilde{m}_e}{\tilde{m}_\mu}+s_22\sqrt{\frac{\tilde{m}_e}{\tilde{m}_\mu}(1-\delta_\ell)\cos\phi_a}\right)}{(1-\delta_\ell)\left(1+s_3\frac{\tilde{m}_e}{\tilde{m}_\mu}\right)(1+s_2\tilde{m}_e)-\frac{1}{2}\frac{\tilde{m}_e}{\tilde{m}_\mu}f_{\ell 1}\left(1-\delta_\ell+\frac{\tilde{m}_\mu}{\tilde{m}_e}+s_12\sqrt{\frac{\tilde{m}_\mu}{\tilde{m}_e}(1-\delta_\ell)\cos\phi_a}\right)}, \quad \varepsilon_{13} = \frac{f_{\ell 1}\left(1-\delta_\ell+\frac{\tilde{m}_\mu}{\tilde{m}_e}+s_12\sqrt{\frac{\tilde{m}_\mu}{\tilde{m}_e}(1-\delta_\ell)\cos\phi_a}\right)}{(1-\delta_\ell)\left(1+s_3\frac{\tilde{m}_e}{\tilde{m}_\mu}\right)(1+s_2\tilde{m}_e)}, \\ \varepsilon_{12} &= \frac{f_{\ell 2}(1+s_3(\delta_\ell-1))+f_{\ell 1}\frac{\tilde{m}_\mu}{\tilde{m}_e}+f_{\ell 1}(1-\delta_\ell)-2s_1f_{\ell 1}\sqrt{\frac{\tilde{m}_\mu}{\tilde{m}_e}(1-\delta_\ell)c_a}+(-1)^i 2\left(\sqrt{(1+s_3(\delta_\ell-1))(1-\delta_\ell)f_{\ell 1}f_{\ell 2}c_c}-s_1\sqrt{\frac{\tilde{m}_\mu}{\tilde{m}_e}(1+s_3(\delta_\ell-1))f_{\ell 1}f_{\ell 2}c_{ac}}\right)}{(1-\delta_\ell)\left(1+s_3\frac{\tilde{m}_e}{\tilde{m}_\mu}\right)(1+s_2\tilde{m}_e)-\frac{\tilde{m}_e}{\tilde{m}_\mu}\frac{f_{\ell 1}}{2}\left(1-\delta_\ell+\frac{\tilde{m}_\mu}{\tilde{m}_e}+s_12\sqrt{\frac{\tilde{m}_\mu}{\tilde{m}_e}(1-\delta_\ell)\cos\phi_a}\right)},\end{aligned}\tag{C3}$$

where $i = 0$ for \mathbf{M}_ℓ^2 , $i = 1$ for \mathbf{M}_ℓ^4 , $c_a = \cos\phi_a$, $c_c = \cos\phi_c$, and $c_{ac} = \cos(\phi_a + \phi_c)$.

2. Parameters of equivalent class with two texture zeros type-II

For the mass matrices \mathbf{M}_ℓ^0 and \mathbf{M}_ℓ^3 ,

$$\begin{aligned}\varepsilon_{23} &= \frac{f_{\ell 1}\delta_\ell+f_{\ell 2}\tilde{\mu}_\ell-2\sqrt{\tilde{\mu}_\ell\delta_\ell f_{\ell 1}f_{\ell 2}\cos\phi_c}}{\tilde{\mu}_\ell\left(1+\frac{\tilde{m}_e}{\tilde{m}_\mu}\right)(1-\tilde{m}_e)-\frac{1}{2}\frac{\tilde{\sigma}_{\ell 1}}{\tilde{m}_\mu}\left(f_{\ell 2}\delta_\ell+\tilde{\mu}_\ell f_{\ell 1}+2\sqrt{\tilde{\mu}_\ell\delta_\ell f_{\ell 1}f_{\ell 2}\cos\phi_c}\right)}, \quad \varepsilon_{13} = \frac{f_{\ell 2}\delta_\ell+\tilde{\mu}_\ell f_{\ell 1}+2\sqrt{\tilde{\mu}_\ell\delta_\ell f_{\ell 1}f_{\ell 2}\cos\phi_c}}{\tilde{\mu}_\ell\left(1+\frac{\tilde{m}_e}{\tilde{m}_\mu}\right)(1-\tilde{m}_e)}, \\ \varepsilon_{12} &= \frac{f_{\ell 2}\delta_\ell+f_{\ell 1}\tilde{\mu}_\ell+f_{\ell 1}\frac{\tilde{\sigma}_{\ell 2}\tilde{\sigma}_{\ell 3}}{\tilde{\sigma}_{\ell 1}}-2\sqrt{\tilde{\mu}_\ell\delta_\ell f_{\ell 1}f_{\ell 2}\cos\phi_c}+(-1)^i 2\sqrt{\frac{\tilde{\sigma}_{\ell 2}\tilde{\sigma}_{\ell 3}}{\tilde{\sigma}_{\ell 1}}\delta_\ell f_{\ell 1}f_{\ell 2}\cos(\phi_a+\phi_c)}+(-1)^{(i+1)}2f_{\ell 1}\sqrt{\frac{\tilde{\sigma}_{\ell 2}\tilde{\sigma}_{\ell 3}}{\tilde{\sigma}_{\ell 1}}\tilde{\mu}_\ell\cos\phi_a}}{\tilde{\mu}_\ell(1-\tilde{m}_e)\left(1+\frac{\tilde{m}_e}{\tilde{m}_\mu}\right)-\frac{\tilde{\sigma}_{\ell 1}}{2\tilde{m}_\mu}\left(f_{\ell 2}\delta_\ell+f_{\ell 1}\tilde{\mu}_\ell+2\sqrt{\tilde{\mu}_\ell\delta_\ell f_{\ell 1}f_{\ell 2}\cos\phi_c}\right)},\end{aligned}\tag{C4}$$

where $i = 0$ for \mathbf{M}_ℓ^0 , $i = 1$ for \mathbf{M}_ℓ^3 . For the mass matrices \mathbf{M}_ℓ^1 and \mathbf{M}_ℓ^5 ,

$$\begin{aligned}\varepsilon_{23} &= \frac{\frac{\tilde{\sigma}_{\ell 1} \tilde{\sigma}_{\ell 3}}{\tilde{\sigma}_{\ell 2}} f_{\ell 2} + \delta_\ell f_{\ell 1} + 2\sqrt{\frac{\tilde{\sigma}_{\ell 1} \tilde{\sigma}_{\ell 3}}{\tilde{\sigma}_{\ell 2}}} \delta_\ell f_{\ell 1} f_{\ell 2} \cos(\phi_a + \phi_c)}{\tilde{\mu}_\ell \left(1 + \frac{\tilde{m}_e}{\tilde{m}_\mu}\right) (1 - \tilde{m}_e) - \frac{1}{2} \frac{\tilde{\sigma}_{\ell 1}}{\tilde{m}_\mu} \left(f_{\ell 2} \delta_\ell + \frac{\tilde{\sigma}_{\ell 2} \tilde{\sigma}_{\ell 3}}{\tilde{\sigma}_{\ell 1}} f_{\ell 1} - 2\sqrt{\frac{\tilde{\sigma}_{\ell 2} \tilde{\sigma}_{\ell 3}}{\tilde{\sigma}_{\ell 1}}} \delta_\ell f_{\ell 1} f_{\ell 2} \cos(\phi_a + \phi_c)\right)}, \quad \varepsilon_{13} = \frac{f_{\ell 2} \delta_\ell + \frac{\tilde{\sigma}_{\ell 2} \tilde{\sigma}_{\ell 3}}{\tilde{\sigma}_{\ell 1}} f_{\ell 1} - 2\sqrt{\frac{\tilde{\sigma}_{\ell 2} \tilde{\sigma}_{\ell 3}}{\tilde{\sigma}_{\ell 1}}} \delta_\ell f_{\ell 1} f_{\ell 2} \cos(\phi_a + \phi_c)}{\tilde{\mu}_\ell \left(1 + \frac{\tilde{m}_e}{\tilde{m}_\mu}\right) (1 - \tilde{m}_e)}, \\ \varepsilon_{12} &= \frac{f_{\ell 2} \delta_\ell + f_{\ell 1} \tilde{\mu}_\ell + f_{\ell 1} \frac{\tilde{\sigma}_{\ell 2} \tilde{\sigma}_{\ell 3}}{\tilde{\sigma}_{\ell 1}} + (-1)^{(i+1)} 2\sqrt{\tilde{\mu}_\ell \delta_\ell f_{\ell 1} f_{\ell 2}} \cos \phi_c + 2\sqrt{\frac{\tilde{\sigma}_{\ell 2} \tilde{\sigma}_{\ell 3}}{\tilde{\sigma}_{\ell 1}}} \delta_\ell f_{\ell 1} f_{\ell 2} \cos(\phi_a + \phi_c) + (-1)^{(i+1)} 2f_{\ell 1} \sqrt{\frac{\tilde{\sigma}_{\ell 2} \tilde{\sigma}_{\ell 3}}{\tilde{\sigma}_{\ell 1}}} \tilde{\mu}_\ell \cos \phi_a}{\tilde{\mu}_\ell (1 - \tilde{m}_e) \left(1 + \frac{\tilde{m}_e}{\tilde{m}_\mu}\right) - \frac{\tilde{\sigma}_{\ell 1}}{2\tilde{m}_\mu} \left(f_{\ell 2} \delta_\ell + f_{\ell 1} \frac{\tilde{\sigma}_{\ell 2} \tilde{\sigma}_{\ell 3}}{\tilde{\sigma}_{\ell 1}} - 2\sqrt{\frac{\tilde{\sigma}_{\ell 2} \tilde{\sigma}_{\ell 3}}{\tilde{\sigma}_{\ell 1}}} \delta_\ell f_{\ell 1} f_{\ell 2} \cos(\phi_a + \phi_c)\right)},\end{aligned}\tag{C5}$$

where $i = 0$ for \mathbf{M}_ℓ^1 , $i = 1$ for \mathbf{M}_ℓ^5 . For the mass matrices \mathbf{M}_ℓ^2 and \mathbf{M}_ℓ^4 ,

$$\begin{aligned}\varepsilon_{23} &= \frac{f_{\ell 2} \left(\tilde{\mu}_\ell + \frac{\tilde{\sigma}_{\ell 1} \tilde{\sigma}_{\ell 3}}{\tilde{\sigma}_{\ell 2}} - 2\sqrt{\tilde{\mu}_\ell \frac{\tilde{\sigma}_{\ell 1} \tilde{\sigma}_{\ell 3}}{\tilde{\sigma}_{\ell 2}}} \cos \phi_a\right)}{\tilde{\mu}_\ell \left(1 + \frac{\tilde{m}_e}{\tilde{m}_\mu}\right) (1 - \tilde{m}_e) - \frac{1}{2} \frac{\tilde{\sigma}_{\ell 1}}{\tilde{m}_\mu} f_{\ell 1} \left(\tilde{\mu}_\ell + \frac{\tilde{\sigma}_{\ell 2} \tilde{\sigma}_{\ell 3}}{\tilde{\sigma}_{\ell 1}} - 2\sqrt{\tilde{\mu}_\ell \frac{\tilde{\sigma}_{\ell 2} \tilde{\sigma}_{\ell 3}}{\tilde{\sigma}_{\ell 1}}} \cos \phi_a\right)}, \quad \varepsilon_{13} = \frac{f_{\ell 1} \left(\tilde{\mu}_\ell + \frac{\tilde{\sigma}_{\ell 2} \tilde{\sigma}_{\ell 3}}{\tilde{\sigma}_{\ell 1}} - 2\sqrt{\tilde{\mu}_\ell \frac{\tilde{\sigma}_{\ell 2} \tilde{\sigma}_{\ell 3}}{\tilde{\sigma}_{\ell 1}}} \cos \phi_a\right)}{\tilde{\mu}_\ell \left(1 + \frac{\tilde{m}_e}{\tilde{m}_\mu}\right) (1 - \tilde{m}_e)}, \\ \varepsilon_{12} &= \frac{f_{\ell 2} \delta_\ell + f_{\ell 1} \tilde{\mu}_\ell + f_{\ell 1} \frac{\tilde{\sigma}_{\ell 2} \tilde{\sigma}_{\ell 3}}{\tilde{\sigma}_{\ell 1}} + (-1)^i 2\sqrt{\tilde{\mu}_\ell \delta_\ell f_{\ell 1} f_{\ell 2}} \cos \phi_c + (-1)^{(i+1)} 2\sqrt{\frac{\tilde{\sigma}_{\ell 2} \tilde{\sigma}_{\ell 3}}{\tilde{\sigma}_{\ell 1}}} \delta_\ell f_{\ell 1} f_{\ell 2} \cos(\phi_a + \phi_c) + 2f_{\ell 1} \sqrt{\frac{\tilde{\sigma}_{\ell 2} \tilde{\sigma}_{\ell 3}}{\tilde{\sigma}_{\ell 1}}} \tilde{\mu}_\ell \cos \phi_a}{\tilde{\mu}_\ell (1 - \tilde{m}_e) \left(1 + \frac{\tilde{m}_e}{\tilde{m}_\mu}\right) - \frac{\tilde{\sigma}_{\ell 1}}{2\tilde{m}_\mu} f_{\ell 1} \left(\tilde{\mu}_\ell + \frac{\tilde{\sigma}_{\ell 2} \tilde{\sigma}_{\ell 3}}{\tilde{\sigma}_{\ell 1}} - 2\sqrt{\tilde{\mu}_\ell \frac{\tilde{\sigma}_{\ell 2} \tilde{\sigma}_{\ell 3}}{\tilde{\sigma}_{\ell 1}}} \cos \phi_a\right)}.\end{aligned}\tag{C6}$$

3. Parameters of equivalent class with two texture zeros type-III

For the mass matrices \mathbf{M}_ℓ^0 and \mathbf{M}_ℓ^3 ,

$$\begin{aligned}\varepsilon_{23} &= \frac{(1+t_\beta^2)(f_{\ell 2}(1-\delta_\ell)+f_{\ell 1}f_{\ell 3})+2\left(f_{\ell 2}t_\beta(1-\delta_\ell)-f_{\ell 1}f_{\ell 3}t_\beta+\mathbf{s}_1\mathbf{s}_2(1-t_\beta^2)\sqrt{f_{\ell 1}f_{\ell 2}f_{\ell 3}(1-\delta_\ell)}\right)\cos\phi_c}{(1+t_\beta^2)(1-\delta_\ell)\left(1+\mathbf{s}_3\frac{\tilde{m}_e}{\tilde{m}_\mu}\right)(1+\mathbf{s}_2\tilde{m}_e)-\frac{1}{2}\frac{\tilde{m}_e}{\tilde{m}_\mu}\left((1+t_\beta^2)(f_{\ell 1}(1-\delta_\ell)+f_{\ell 2}f_{\ell 3})+2\left(t_\beta(f_{\ell 1}(1-\delta_\ell)-f_{\ell 2}f_{\ell 3})-\sqrt{(1-\delta_\ell)f_{\ell 1}f_{\ell 2}f_{\ell 3}}\right)\cos\phi_c\right)}, \\ \varepsilon_{13} &= \frac{(1+t_\beta^2)(f_{\ell 1}(1-\delta_\ell)+f_{\ell 2}f_{\ell 3})+2\left(t_\beta(f_{\ell 1}(1-\delta_\ell)-f_{\ell 2}f_{\ell 3})-\sqrt{(1-\delta_\ell)f_{\ell 1}f_{\ell 2}f_{\ell 3}}\right)\cos\phi_c}{(1+t_\beta^2)(1-\delta_\ell)\left(1+\mathbf{s}_3\frac{\tilde{m}_e}{\tilde{m}_\mu}\right)(1+\mathbf{s}_2\tilde{m}_e)}, \\ \varepsilon_{12} &= \frac{\left(\sqrt{f_{\ell 2}f_{\ell 3}t_\beta}+\sqrt{f_{\ell 1}(1-\delta_\ell)}\right)^2+\left(\sqrt{f_{\ell 2}f_{\ell 3}}-t_\beta\sqrt{f_{\ell 1}(1-\delta_\ell)}\right)^2+2\left(\sqrt{f_{\ell 2}f_{\ell 3}t_\beta}+\sqrt{f_{\ell 1}(1-\delta_\ell)}\right)\left(\sqrt{f_{\ell 2}f_{\ell 3}}-t_\beta\sqrt{f_{\ell 1}(1-\delta_\ell)}\right)c_c}{(1+t_\beta^2)(1-\delta_\ell)\left(1+\mathbf{s}_3\frac{\tilde{m}_e}{\tilde{m}_\mu}\right)(1+\mathbf{s}_2\tilde{m}_e)-N\varepsilon_{13}} \times \\ &\quad \times \frac{+\frac{\tilde{m}_\mu}{\tilde{m}_e}(1+t_\beta^2)f_{\ell 1}+(-1)^i2\mathbf{s}_1\sqrt{\frac{\tilde{m}_\mu}{\tilde{m}_e}(1+t_\beta^2)f_{\ell 1}}\left(\sqrt{f_{\ell 2}f_{\ell 3}t_\beta}+\sqrt{f_{\ell 1}(1-\delta_\ell)}\right)c_a+(-1)^i2\mathbf{s}_1\sqrt{\frac{\tilde{m}_\mu}{\tilde{m}_e}(1+t_\beta^2)f_{\ell 1}}\left(\sqrt{f_{\ell 2}f_{\ell 3}}-t_\beta\sqrt{f_{\ell 1}(1-\delta_\ell)}\right)c_{ac}}{N\varepsilon_{13}},\end{aligned}\tag{C7}$$

where $i = 0$ for \mathbf{M}_ℓ^0 , $i = 1$ for \mathbf{M}_ℓ^3 , $c_a = \cos \phi_a$, $c_c = \cos \phi_c$, $c_{ac} = \cos(\phi_a + \phi_c)$, and $t_\beta = \tan \beta$,

$$N\varepsilon_{13} = (1+t_\beta^2)(f_{\ell 1}(1-\delta_\ell)+f_{\ell 2}f_{\ell 3})+2\left(t_\beta(f_{\ell 1}(1-\delta_\ell)-f_{\ell 2}f_{\ell 3})-\sqrt{(1-\delta_\ell)f_{\ell 1}f_{\ell 2}f_{\ell 3}}\right)\cos\phi_c.\tag{C8}$$

For the mass matrices \mathbf{M}_ℓ^1 and \mathbf{M}_ℓ^5 ,

$$\begin{aligned}\varepsilon_{23} &= \frac{\frac{\tilde{m}_e}{\tilde{m}_\mu}f_{\ell 2}(1+t_\beta^2)+f_{\ell 1}f_{\ell 3}+f_{\ell 2}t_\beta^2(1-\delta_\ell)+\mathbf{s}_1\mathbf{s}_2t_\beta\sqrt{f_{\ell 1}f_{\ell 2}f_{\ell 3}(1-\delta_\ell)}+2\sqrt{1+t_\beta^2}\sqrt{\frac{\tilde{m}_e}{\tilde{m}_\mu}}\left(\mathbf{s}_1\sqrt{f_{\ell 1}f_{\ell 2}f_{\ell 3}}+\mathbf{s}_2t_\beta\sqrt{1-\delta_\ell}\right)\cos(\phi_a+\phi_c)}{(1+t_\beta^2)(1-\delta_\ell)\left(1+\mathbf{s}_3\frac{\tilde{m}_e}{\tilde{m}_\mu}\right)(1+\mathbf{s}_2\tilde{m}_e)-N\varepsilon_{13}}, \\ \varepsilon_{13} &= \frac{(1+t_\beta^2)\frac{\tilde{m}_\mu}{\tilde{m}_e}f_{\ell 1}+f_{\ell 2}f_{\ell 3}+f_{\ell 1}t_\beta^2(1-\delta_\ell)-2t_\beta\sqrt{f_{\ell 1}f_{\ell 2}f_{\ell 3}(1-\delta_\ell)}-2\mathbf{s}_1\sqrt{1+t_\beta^2}\sqrt{\frac{\tilde{m}_\mu}{\tilde{m}_e}}\left(\sqrt{f_{\ell 1}f_{\ell 2}f_{\ell 3}}-t_\beta f_{\ell 1}\sqrt{1-\delta_\ell}\right)\cos(\phi_a+\phi_c)}{(1+t_\beta^2)(1-\delta_\ell)\left(1+\mathbf{s}_3\frac{\tilde{m}_e}{\tilde{m}_\mu}\right)(1+\mathbf{s}_2\tilde{m}_e)}, \\ \varepsilon_{12} &= \frac{\left(\sqrt{f_{\ell 2}f_{\ell 3}t_\beta}+\sqrt{f_{\ell 1}(1-\delta_\ell)}\right)^2+\left(\sqrt{f_{\ell 2}f_{\ell 3}}-t_\beta\sqrt{f_{\ell 1}(1-\delta_\ell)}\right)^2+(-1)^j2c_c\left(\sqrt{f_{\ell 2}f_{\ell 3}t_\beta}+\sqrt{f_{\ell 1}(1-\delta_\ell)}\right)\left(\sqrt{f_{\ell 2}f_{\ell 3}}-t_\beta\sqrt{f_{\ell 1}(1-\delta_\ell)}\right)}{(1+t_\beta^2)(1-\delta_\ell)\left(1+\mathbf{s}_3\frac{\tilde{m}_e}{\tilde{m}_\mu}\right)(1+\mathbf{s}_2\tilde{m}_e)-N\varepsilon_{13}} \times \\ &\quad \times \frac{+\frac{\tilde{m}_\mu}{\tilde{m}_e}(1+t_\beta)f_{\ell 1}+(-1)^j2\mathbf{s}_1\sqrt{\frac{\tilde{m}_\mu}{\tilde{m}_e}(1+t_\beta)f_{\ell 1}}\left(\sqrt{f_{\ell 2}f_{\ell 3}t_\beta}+\sqrt{f_{\ell 1}(1-\delta_\ell)}\right)c_a+2\mathbf{s}_1\sqrt{\frac{\tilde{m}_\mu}{\tilde{m}_e}(1+t_\beta)f_{\ell 1}}\left(\sqrt{f_{\ell 2}f_{\ell 3}}-t_\beta\sqrt{f_{\ell 1}(1-\delta_\ell)}\right)c_{ac}}{N\varepsilon_{13}},\end{aligned}\tag{C9}$$

where $i = 0$ for \mathbf{M}_ℓ^1 , $i = 1$ for \mathbf{M}_ℓ^5 , $c_a = \cos \phi_a$, $c_c = \cos \phi_c$, $c_{ac} = \cos(\phi_a + \phi_c)$, $t_\beta = \tan \beta$, and

$$\begin{aligned}N\varepsilon_{13} &= \frac{1}{2}\frac{\tilde{m}_e}{\tilde{m}_\mu}\left(\left(1+t_\beta^2\right)\frac{\tilde{m}_\mu}{\tilde{m}_e}f_{\ell 1}+f_{\ell 2}f_{\ell 3}+f_{\ell 1}t_\beta^2(1-\delta_\ell)-2t_\beta\sqrt{f_{\ell 1}f_{\ell 2}f_{\ell 3}(1-\delta_\ell)}\right. \\ &\quad \left.-2\mathbf{s}_1\sqrt{1+t_\beta^2}\sqrt{\frac{\tilde{m}_\mu}{\tilde{m}_e}}\left(\sqrt{f_{\ell 1}f_{\ell 2}f_{\ell 3}}-t_\beta f_{\ell 1}\sqrt{1-\delta_\ell}\right)\cos(\phi_a+\phi_c)\right).\end{aligned}\tag{C10}$$

For \mathbf{M}_ℓ^2 and \mathbf{M}_ℓ^4

$$\begin{aligned}
\varepsilon_{13} &= \frac{(1+t_\beta^2) \frac{\tilde{m}_\mu}{\tilde{m}_e} f_{\ell 1} + f_{\ell 2} f_{\ell 3} t_\beta^2 + f_{\ell 1} (1-\delta_\ell) + 2t_\beta \sqrt{(1-\delta_\ell) f_{\ell 1} f_{\ell 2} f_{\ell 3}} + 2s_1 \sqrt{1+t_\beta^2} \sqrt{\frac{\tilde{m}_\mu}{\tilde{m}_e}} (t_\beta \sqrt{f_{\ell 1} f_{\ell 2} f_{\ell 3}} + f_{\ell 1} \sqrt{(1-\delta_\ell)}) \cos \phi_a}{(1+t_\beta^2)(1-\delta_\ell) \left(1+s_3 \frac{\tilde{m}_e}{\tilde{m}_\mu}\right) (1+s_2 \tilde{m}_e)}, \\
\varepsilon_{23} &= \frac{f_{\ell 2} \left(\frac{\tilde{m}_e}{\tilde{m}_\mu} (1+t_\beta^2) + 1 - \delta_\ell\right) + f_{\ell 1} f_{\ell 3} t_\beta^2 - 2s_1 s_2 t_\beta \sqrt{\frac{\tilde{m}_e}{\tilde{m}_\mu} f_{\ell 1} f_{\ell 2} f_{\ell 3} (1-\delta_\ell)} + 2 \sqrt{\frac{\tilde{m}_e}{\tilde{m}_\mu}} (1+t_\beta^2) (s_2 f_{\ell 2} \sqrt{1-\delta_\ell} - s_1 t_\beta \sqrt{f_{\ell 1} f_{\ell 2} f_{\ell 3}}) \cos \phi_a}{(1+t_\beta^2)(1-\delta_\ell) \left(1+s_3 \frac{\tilde{m}_e}{\tilde{m}_\mu}\right) (1+s_2 \tilde{m}_e) - N\varepsilon_{13}}, \\
\varepsilon_{12} &= \frac{\left(\sqrt{f_{\ell 2} f_{\ell 3} t_\beta} + \sqrt{f_{\ell 1} (1-\delta_\ell)}\right)^2 + \left(\sqrt{f_{\ell 2} f_{\ell 3}} - t_\beta \sqrt{f_{\ell 1} (1-\delta_\ell)}\right)^2 + (-1)^{i+1} 2 \left(\sqrt{f_{\ell 2} f_{\ell 3} t_\beta} + \sqrt{f_{\ell 1} (1-\delta_\ell)}\right) \left(\sqrt{f_{\ell 2} f_{\ell 3}} - t_\beta \sqrt{f_{\ell 1} (1-\delta_\ell)}\right) c_c}{(1+t_\beta^2)(1-\delta_\ell) \left(1+s_3 \frac{\tilde{m}_e}{\tilde{m}_\mu}\right) (1+s_2 \tilde{m}_e) - N\varepsilon_{13}} \times \\
&\quad \times \frac{+ \frac{\tilde{m}_\mu}{\tilde{m}_e} (1+t_\beta) f_{\ell 1} - 2s_1 \sqrt{\frac{\tilde{m}_\mu}{\tilde{m}_e} (1+t_\beta) f_{\ell 1}} \left(\sqrt{f_{\ell 2} f_{\ell 3} t_\beta} + \sqrt{f_{\ell 1} (1-\delta_\ell)}\right) c_a - 2s_1 \sqrt{\frac{\tilde{m}_\mu}{\tilde{m}_e} (1+t_\beta) f_{\ell 1}} \left(\sqrt{f_{\ell 2} f_{\ell 3}} - t_\beta \sqrt{f_{\ell 1} (1-\delta_\ell)}\right) c_{ac}}{,}
\end{aligned} \tag{C11}$$

where $i = 0$ for \mathbf{M}_ℓ^2 , $i = 1$ for \mathbf{M}_ℓ^4 , $c_a = \cos \phi_a$, $c_c = \cos \phi_c$, $c_{ac} = \cos(\phi_a + \phi_c)$, $t_\beta = \tan \beta$, and

$$\begin{aligned}
N\varepsilon_{13} &= \frac{1}{2} \frac{\tilde{m}_e}{\tilde{m}_\mu} \left(\left(1+t_\beta^2\right) \frac{\tilde{m}_\mu}{\tilde{m}_e} f_{\ell 1} + f_{\ell 2} f_{\ell 3} t_\beta^2 + f_{\ell 1} (1-\delta_\ell) + 2t_\beta \sqrt{(1-\delta_\ell) f_{\ell 1} f_{\ell 2} f_{\ell 3}} \right. \\
&\quad \left. + 2s_1 \sqrt{1+t_\beta^2} \sqrt{\frac{\tilde{m}_\mu}{\tilde{m}_e}} \left(t_\beta \sqrt{f_{\ell 1} f_{\ell 2} f_{\ell 3}} + f_{\ell 1} \sqrt{(1-\delta_\ell)} \right) \cos \phi_a \right).
\end{aligned} \tag{C12}$$

4. Parameters of equivalent class with two texture zeros type-IV

For the mass matrices \mathbf{M}_ℓ^0 and \mathbf{M}_ℓ^3 ,

$$\varepsilon_{13} = \frac{\tilde{m}_\mu}{\tilde{m}_e} \frac{\tilde{f}_\ell - \tilde{m}_e}{\tilde{m}_\mu - \tilde{m}_e}, \quad \varepsilon_{23} = \frac{\tilde{m}_\mu - \tilde{f}_\ell}{\tilde{m}_\mu - \frac{1}{2}\tilde{m}_e - \frac{1}{2}\tilde{f}_\ell}, \quad \varepsilon_{12} = \frac{\tilde{m}_\mu - \tilde{m}_e + (-1)^{i+1} 2 \sqrt{(\tilde{f}_\ell - \tilde{m}_e)(\tilde{m}_\mu - \tilde{f}_\ell)} \cos \phi_a}{\tilde{m}_\mu - \frac{\tilde{m}_e}{2} - \frac{\tilde{f}_\ell}{2}}. \tag{C13}$$

For the mass matrices \mathbf{M}_ℓ^1 and \mathbf{M}_ℓ^5 ,

$$\varepsilon_{13} = \frac{\tilde{m}_\mu}{\tilde{m}_e} \frac{\tilde{m}_\mu - \tilde{f}_\ell}{\tilde{m}_\mu - \tilde{m}_e}, \quad \varepsilon_{23} = \frac{\tilde{f}_\ell - \tilde{m}_e}{\frac{1}{2}\tilde{m}_\mu - \tilde{m}_e + \frac{1}{2}\tilde{f}_\ell}, \quad \varepsilon_{12} = \frac{\tilde{m}_\mu - \tilde{m}_e + (-1)^{i+1} 2 \sqrt{(\tilde{f}_\ell - \tilde{m}_e)(\tilde{m}_\mu - \tilde{f}_\ell)} \cos \phi_a}{\frac{\tilde{m}_\mu}{2} - \tilde{m}_e - \frac{\tilde{f}_\ell}{2}}. \tag{C14}$$

For \mathbf{M}_ℓ^2 and \mathbf{M}_ℓ^4

$$\varepsilon_{13} = \frac{\tilde{m}_\mu}{\tilde{m}_e} \left(1 - 2 \frac{\sqrt{(\tilde{f}_\ell - \tilde{m}_e)(\tilde{m}_\mu - \tilde{f}_\ell)}}{\tilde{m}_\mu - \tilde{m}_e} \cos \phi_a \right), \quad \varepsilon_{23} = \varepsilon_{12} = \frac{\tilde{m}_\mu - \tilde{m}_e + 2 \sqrt{(\tilde{f}_\ell - \tilde{m}_e)(\tilde{m}_\mu - \tilde{f}_\ell)} \cos \phi_a}{\frac{1}{2}(\tilde{m}_\mu - \tilde{m}_e) + \sqrt{(\tilde{f}_\ell - \tilde{m}_e)(\tilde{m}_\mu - \tilde{f}_\ell)} \cos \phi_a}. \tag{C15}$$

Acknowledgments

This work has been partially supported by *CONACYT-SNI (México)*.

-
- [1] T. Ohlsson, Nuclear Physics B **908**, 1 (2016), ISSN 0550-3213, neutrino Oscillations: Celebrating the Nobel Prize in Physics 2015, URL <https://www.sciencedirect.com/science/article/pii/S0550321316300621>.
- [2] Y. Abe et al. (Double Chooz), Phys. Rev. Lett. **108**, 131801 (2012), 1112.6353.
- [3] F. P. An et al. (Daya Bay), Phys. Rev. Lett. **108**, 171803 (2012), 1203.1669.
- [4] J. K. Ahn et al. (RENO), Phys. Rev. Lett. **108**, 191802 (2012), 1204.0626.
- [5] P. F. de Salas, D. V. Forero, S. Gariazzo, P. Martínez-Miravé, O. Mena, C. A. Ternes, M. Tórtola, and J. W. F. Valle, Journal of High Energy Physics **2021** (2021), ISSN 1029-8479, URL [http://dx.doi.org/10.1007/JHEP02\(2021\)071](http://dx.doi.org/10.1007/JHEP02(2021)071).

- [6] P. Zyla et al. (Particle Data Group), PTEP **2020**, 083C01 (2020).
- [7] M. S. Athar et al. (2021), 2111.07586.
- [8] P. F. Harrison, D. H. Perkins, and W. G. Scott, Phys. Lett. B **530**, 167 (2002), hep-ph/0202074.
- [9] Y. Ahn, H.-Y. Cheng, and S. Oh, Phys. Lett. B **715**, 203 (2012), 1105.4460.
- [10] P. Chen, S. Centelles Chuliá, G.-J. Ding, R. Srivastava, and J. W. Valle, Phys. Rev. D **98**, 055019 (2018), 1806.03367.
- [11] K. Hochmuth, S. Petcov, and W. Rodejohann, Phys. Lett. B **654**, 177 (2007), 0706.2975.
- [12] W. Rodejohann and J. Valle, Phys. Rev. D **84**, 073011 (2011), 1108.3484.
- [13] E. Barradas-Guevara, O. Felix-Beltran, F. Gonzalez-Canales, and M. Zeleny-Mora, Phys. Rev. D **97**, 035003 (2018), 1704.03474.
- [14] M. H. Rahat, P. Ramond, and B. Xu, Physical Review D **98** (2018), URL <https://doi.org/10.1103/PhysRevD.98.055030>.
- [15] W. H. Furry, Phys. Rev. **56**, 1184 (1939).
- [16] C. Brofferio, O. Cremonesi, and S. Dell’Oro, Frontiers in Physics **7**, 86 (2019), ISSN 2296-424X, URL <https://www.frontiersin.org/article/10.3389/fphy.2019.00086>.
- [17] H. Fritzsch and Z.-z. Xing, Prog. Part. Nucl. Phys. **45**, 1 (2000), hep-ph/9912358.
- [18] F. Gonzalez Canales, A. Mondragon, and M. Mondragon, Fortsch. Phys. **61**, 546 (2013), 1205.4755.
- [19] A. Gando et al. (KamLAND-Zen), Phys. Rev. Lett. **117**, 082503 (2016), [Addendum: Phys.Rev.Lett. 117, 109903 (2016)], 1605.02889.
- [20] J. B. Albert et al. (EXO), Phys. Rev. Lett. **120**, 072701 (2018), 1707.08707.
- [21] P. A. R. Ade et al. (Planck), Astron. Astrophys. **594**, A13 (2016), 1502.01589.
- [22] H. Georgi, *Lie algebras in particle physics*, vol. 54 (Perseus Books, Reading, MA, 1999), 2nd ed.
- [23] H. Ishimori, T. Kobayashi, H. Ohki, Y. Shimizu, H. Okada, and M. Tanimoto, Prog. Theor. Phys. Suppl. **183**, 1 (2010), 1003.3552.
- [24] F. F. González Canales, Ph.D. thesis, Universidad Nacional Autónoma de México (2011), URL http://oreon.dgbiblio.unam.mx/F/?func=service&doc_library=TES01&doc_number=000674715&line_number=0001&func_code=WEB-BRIEF&service_type=MEDIA.